TRENDS IN SCIENCES 2026; 23(10): 13412
https://doi.org/10.48048/tis.2026.13412
RESEARCH ARTICLE

Antioxidant Capacity and Acetylcholinesterase Inhibitory Activity of Ethanolic Rhizome Extract of *Curcuma xanthorrhiza*: An Integrated *in Vitro* and *in Silico* Study

Faishal Ahmad Arbi[1], Dimas Andrianto[2], Dewi Anggraini Septaningsih[3,5], Ukhradiya Magharaniq Safira Purwanto[2], Rini Kurniasih[4] and Mega Safithri[2,5,*]

[1]*Biochemistry Master's Program, Faculty of Mathematics and Natural Sciences, Bogor Agricultural University, Bogor, Indonesia*
[2]*Division of Bioanalysis, Department Biochemistry, Faculty of Mathematics and Natural Sciences, Bogor Agricultural University, Bogor, Indonesia*
[3]*Department Chemistry, Faculty of Mathematics and Natural Sciences, Indonesia Defence University, Bogor, Indonesia*
[4]*Division of Biomolecules, Department Biochemistry, Faculty of Mathematics and Natural Sciences, Bogor Agricultural University, Bogor, Indonesia*
[5]*Tropical Biopharmaca Research Center, Bogor, Indonesia*

([*]Corresponding author's e-mail: safithri@apps.ipb.ac.id)

Received: 21 January 2026, Revised: 4 March 2026, Accepted: 15 March 2026, Published: 20 April 2026

Abstract

Alzheimer's disease (AD) is the leading cause of dementia and is characterized by progressive memory loss and cognitive decline. A key pathological mechanism involves excessive hydrolysis of acetylcholine by acetylcholinesterase (AChE), resulting in impaired cholinergic neurotransmission. Therefore, AChE remains a major therapeutic target. Curcuma xanthorrhiza rhizome contains diverse bioactive compounds with reported neuroprotective potential. This study presents the first integrated metabolomics-bioactivity-ADMET workflow applied to ethanolic *C. xanthorrhiza* extract to systematically identify potential natural AChE inhibitors. Secondary metabolites, including total phenolics, flavonoids, tannins, and alkaloids, were quantified by colorimetric methods. Antioxidant capacity was evaluated using DPPH, FRAP, and lipid peroxidation inhibition assays. Metabolite profiling was conducted by UHPLC-Q-Orbitrap-HRMS, and AChE inhibitory activity was assessed using the Ellman method, with donepezil as the reference drug. Molecular docking against AChE (PDB ID: 6O4W) and *in silico* ADMET prediction were performed to elucidate binding interactions and pharmacokinetic suitability. The extract exhibited strong antioxidant activity and significant AChE inhibition (IC_{50} 46.63 µg/mL), while donepezil showed very strong inhibition (IC_{50} 0.03 µg/mL). Metabolomic analysis identified 43 compounds, predominantly curcuminoids and sesquiterpenes, with xanthorrhizol quantified as a major constituent. Docking analysis revealed several high-affinity ligands; bisdemethoxycurcumin showed the strongest binding energy (ΔGbind −11.55 kcal/mol) but less favorable ADMET properties. In contrast, xanthorrhizol (ΔGbind −8.63 kcal/mol) demonstrated balanced binding interactions and a more favorable predicted pharmacokinetic profile. Overall, this integrative approach enables rational prioritization of bioactive constituents from complex plant extracts and highlights xanthorrhizol as a promising candidate for further experimental validation as a natural AChE inhibitor.

Keywords: Acetylcholinesterase inhibitors, Alzheimer's disease, Bioactive compounds, Curcuma xanthorrhiza, Molecular docking, Pharmacokinetics

Introduction

Dementia is a progressive neurodegenerative disorder marked by a decline in cognitive functions, such as memory and behavior, resulting from structural and functional changes in the brain. The likelihood of developing dementia rises sharply with age, making older adults the most at-risk group [1]. Oxidative stress significantly contributes to neurodegeneration by increasing reactive oxygen species, which damage neurons, impair mitochondrial function, and hasten Alzheimer's disease progression, the primary cause of dementia [2]. According to WHO data, approximately 55 million people currently exhibit dementia symptoms. This number is projected to grow to 82 million by 2030 and 152 million by 2050, predominantly in developing nations. Addressing this growing burden calls for effective, affordable strategies for prevention and treatment [3].

Dementia is divided into several types, namely Alzheimer's Disease (AD) and Vascular Dementia (VD) [1]. These 2 types of dementia contribute significantly to disability and mortality in the elderly [2]. One of the main pathophysiology in Alzheimer's disease is acetylcholine deficiency. Acetylcholine is a crucial neurotransmitter involved in memory enhancement in the brain. In people with dementia, acetylcholine undergoes overdegradation due to increased activity of its key metabolic enzyme, acetylcholinesterase. This increased degradation triggers the termination of cholinergic signal transmission at brain neuron synapses. One common approach to prevention and treatment is the consumption of drugs that effectively inhibit the acetylcholinesterase (AChE) enzyme [4]. AChE inhibition has become the main pharmacological strategy in the treatment of AD due to its potential to increase acetylcholine levels in the brain and improve cognitive function [5].

Synthetic drugs such as donepezil, rivastigmine, and galantamine have been clinically approved as AChE inhibitors. However, long-term use of these drugs causes serious side effects such as gastrointestinal disorders, dizziness, insomnia, and bradycardia [6]. Although some studies have shown the effectiveness of donepezil in improving the cognitive function of patients, the therapeutic effectiveness of this drug is only symptomatic and cannot stop the progression of Alzheimer's disease [7]. This has encouraged the design of safer alternative drugs with long-term protective effects using natural sources or traditional medicinal plants.

In recent years, numerous studies have reported the potential of herbal extracts and plant-derived compounds as AChE inhibitors, combined *in silico* and *in vitro* approaches. Safithri *et al*. [8] demonstrated that bioactive compounds from *Piper crocatum* exhibited significant AChE inhibitory activity, supported by molecular docking analysis and enzymatic assays, highlighting the effectiveness of integrating computational and experimental methods in screening natural AChE inhibitors [8]. Similar approaches have been applied to various medicinal plants, confirming that phytochemicals such as alkaloids, flavonoids, phenolics, and terpenoids can interact favorably with the AChE active site and contribute to neuroprotective effects [9,10].

Indonesia has great potential in the development of herbal medicines through its biodiversity in terms of flora. One traditional plant that has strong potential as an anti-Alzheimer's agent is turmeric (*C. xanthorrhiza*), which has been scientifically used as an anti-inflammatory, hepatoprotection, and antioxidant. *C. xanthorrhiza* contains various active compounds such as xanthorrhizol, curcumin, and germacrone, which have been reported to have neuroprotective and antioxidant activities which has the potential to be a natural AChE inhibitor [11]. The antioxidant activity in *C. xanthorrhiza* can also inhibit the occurrence of further oxidative stress that contributes to the pathogenesis of AD neurodegenerative disease [12].

Although previous studies have reported antioxidant and neuroprotective properties of *Curcuma xanthorrhiza* and related Curcuma species, most investigations focused either on isolated compounds or on limited bioactivity assays without comprehensive metabolite profiling. Moreover, studies linking high-resolution metabolomics data with enzyme inhibition assays and subsequent pharmacokinetic-toxicological (ADMET) prediction remain scarce. In particular, there is a lack of systematic workflows that integrate untargeted UHPLC-Q-Orbitrap-HRMS metabolite identification with *in vitro* AChE inhibition data to rationally prioritize active compounds from complex

plant extracts. This study evaluated ethanolic extract of *C. xanthorrhiza* rhizome as a candidate natural AChE inhibitor using an integrated chemical, biological, and computational approach.

Materials and methods

Preparation of *Curcuma xanthorrhiza* rhizome extract

The *Curcuma xanthorrhiza* rhizomes were obtained from Sukabumi, West Java, Indonesia. The rhizomes were harvested at 6 months after plantation and washed thoroughly. The samples were dried in an oven at 50 °C for 3 days. Once dry, the samples were ground into powder and sieved using a 60-mesh sieve. The resulting powder was then extracted using 70% ethanol solvent (1:10) (b:v) for 24 h at room temperature. The extract was filtered, and the powder residue was re-macerated with 100 mL of ethanol up to 3 times. The collected filtrate was concentrated with a vacuum rotary evaporator to obtain a *C. xanthorrhiza* ethanolic extract [13,14]. The extract yield was expressed as a percentage using the following equation:

$$\text{Yield (\%)} = \left\{\frac{\text{extract weights}}{[\text{simplicia weights} \times (1 - \text{moisture content})]}\right\} \times 100\% \quad [13]$$

Quantification of secondary metabolite content

Total phenolic content (TPC) was determined using the Folin-Ciocalteu method. Briefly, 20 µL of sample extract or gallic acid standard solution was mixed with 120 µL of 10% (v/v) Folin-Ciocalteu reagent in a 96-well microplate. After homogenization, 80 µL of 7.5% (w/v) Na_2CO_3 solution was added. The reaction mixture was incubated for 30 min in the dark at room temperature, and the absorbance was measured at 750 nm using a microplate reader (SPECTROstar® Nano, BMG LABTECH). Gallic acid was used as the calibration standard at concentrations of 0, 30, 45, 60, 75, 90, 105, and 120 mg/L. TPC was expressed as mg gallic acid equivalent (GAE) per g of extract [14].

Total flavonoid content (TFC) was determined using the aluminum chloride colorimetric method. A volume of 10 µL of sample extract was mixed with 50 µL of 99.8% ethanol, 10 µL of 10% (w/v) $AlCl_3$, 10 µL of 1 mol/L potassium acetate (CH_3COOK), and 120 µL of distilled water. The mixture was incubated at room temperature for 30 min, after which the absorbance was measured at 415 nm using a microplate reader (SPECTROstar® Nano, BMG LABTECH). Quercetin was used as the reference standard at concentrations of 0, 150, 200, 250, 300, 350, 400, and 450 mg/L. TFC was expressed as mg quercetin equivalent (QE) per g of extract [15].

Total tannin content (TTC) was analyzed using the Folin-Ciocalteu method with tannic acid as standard. Twenty microliters of sample extract or tannic acid solution was mixed with 120 µL of 10% (v/v) Folin-Ciocalteu reagent in a 96-well microplate and allowed to stand for 5 min at room temperature. Subsequently, 80 µL of 10% (w/v) Na_2CO_3 solution was added. The mixture was homogenized and incubated for 30 min in the dark, after which the absorbance was measured at 669 nm using a microplate reader (SPECTROstar® Nano, BMG LABTECH). The calibration curve was prepared using tannic acid at concentrations of 0, 12.5, 25, 37.5, 50, 62.5, 75, 87.5, and 100 mg/L. TTC was expressed as mg tannic acid equivalent (TAE) per g of extract [16].

Total alkaloid content (TAC) was determined according to the method described by previous research with minor modifications. Briefly, 2 mL of sample solution was mixed with 1 mL of 2 N HCl, followed by extraction with 3 mL of chloroform. The chloroform phase was discarded, and 2 mL of 0.1 N NaOH was added to the remaining aqueous phase. Subsequently, 2 mL of phosphate buffer (pH 4.7) and 2 mL of bromocresol green (BCG) solution were added, and the mixture was extracted with 3 mL of chloroform 3 times. The combined chloroform extracts were collected, and the absorbance was measured at 470 nm. Caffeine was used as the reference standard at concentrations of 0, 100, 200, 300, 400, 500, 600, 700, and 800 mg/L. TAC was expressed as mg caffeine equivalent (CE) per g of extract [17]. The concentration of secondary metabolites was calculated using the linear regression equation obtained from the corresponding standard calibration curves and expressed as equivalents per gram of extract. Quantification of secondary metabolite content is calculated using the formula [14-17]:

$$\text{TPC/TFC/TTC/TAC} = \left\{\frac{[C_{standard}] \times V}{m}\right\} \times \text{DF}$$

where, C = Concentration of standard; m = Mass; V = Volume; DF = Dilution factor

Antioxidant capacity using the DPPH and FRAP method

The antioxidant activity of the extracts was evaluated using the DPPH radical scavenging assay. Briefly, 100 µL of sample extract was mixed with 100 µL of DPPH solution (125 µmol/L in ethanol) in a 96-well microplate. The mixture was incubated in the dark at room temperature for 30 min. The absorbance was then measured at 515 nm using a microplate reader. Trolox was used as a positive control at concentrations of 0, 20, 30, 40, 50, 60, 70, and 80 µM. The antioxidant activity was expressed as Trolox Equivalent Antioxidant Capacity (TEAC) and reported as µmol Trolox equivalent (TE) per g of extract [14].

The ferric reducing antioxidant power (FRAP) assay was conducted according to a previously reported method with slight modifications. The FRAP reagent was freshly prepared by mixing 300 mmol/L acetate buffer (pH 3.6), 10 mmol/L TPTZ solution, and 20 mmol/L $FeCl_3$ solution in a volume ratio of 10:1:1 (v/v/v). Trolox standard solutions were prepared in 70% ethanol at concentrations of 0, 100, 150, 200, 250, 300, 350, and 400 µM. For the assay, 20 µL of sample extract was added to 180 µL of FRAP reagent in a 96-well microplate. The mixture was incubated at 37 °C for 15 min, after which the absorbance was measured at 595 nm using a microplate reader [18]. The FRAP value was expressed as µmol Trolox equivalent (TE) per g of extract. The antioxidant capacity was calculated using the following equation [14-18]:

$$\text{Antioxidant Capacity} = \left\{\frac{[C_{trolox}] \times \text{V}}{m}\right\} \times \text{DF}$$

where, C = Concentration of Trolox; V = Volume; m = Mass; DF = Dilution factor

Lipid antioxidant capacity using the TBA method

Malondialdehyde (MDA) concentration analysis was performed by preparing TMP standard solutions with concentrations of 0, 2.5, 5, 7.5, 10, 12.5, 15, 17.5, 20, 22.5, 25, 27.5, 30, and 32.5 µM. The positive control used was 200 mg/L alpha-tocopherol, while the negative controls and sample solutions had concentrations of 0, 100, 200, 500, and 1,000 mg/L. Each solution (standard, positive control, and sample) was taken in 1 mL, then 2 mL of 0.1 M phosphate buffer pH 7, and 2 mL of 50 mM linoleic acid in 99.8% ethanol were added. The mixture was placed in a dark bottle and incubated at 40 °C for the maximum incubation time obtained. Each mixture was taken in 1 mL portions, then 2 mL of 20% TCA (w/v) and 2 mL of 1% TBA solution (w/v) in 50% acetic acid (v/v) were added. The mixture was incubated at 100 °C for 10 min and centrifuged at 3,000 rpm for 15 min, then measured at a wavelength of 532 nm [19,20]. The percentage of inhibition of the extract is calculated using the following formula [20]:

$$\text{Inhibition} = \left\{\frac{(\text{[MDA] negative control - [MDA] extract})}{\text{[MDA] negative control}}\right\} \times 100\%$$

Identification of active compound content using liquid chromatography-mass spectometry

Analysis of the active compounds in the ethanol extract of *C. xanthorrhiza* rhizome was performed using a Vanquish UHPLC instrument combined with a Q Exactive Plus Orbitrap HRMS mass spectrometer (Thermo Scientific). A total of 5 mg of 70% ethanol extract of temulawak rhizome was dissolved in 1 mL of methanol, then filtered using a 0.2 µm nylon membrane before being injected into the chromatography system. Separation was performed on an Accucore C18 column (100×2.1 mm^2; 1.5 µm) at a flow rate of 0.2 mL/min. The elution system consisted of 2 phases: Water containing 0.1% formic acid (phase A) and acetonitrile with 0.1% formic acid (phase B). The gradient used was 0 - 1 min (5% B), 1 - 25 min (5% - 95% B), 25 - 28 min (95% B), and 28 - 33 min (5% B). The column temperature was set at 30 °C with an injection volume of 2 µL. Mass spectra were obtained in the m/z range of 100 - 1,500 in positive ionization mode. The analysis data were then processed using the PubChem and literature online databases for compound identification [21].

Acetylcholinesterase inhibition using Ellman's method

The inhibition of acetylcholinesterase (AChE) activity of *C. xanthorrhiza* rhizome extract was evaluated at varying concentrations (0.1, 1, 5, 10, 20, 30, 40, 50 and 60 µg/L) using a commercial colorimetric acetylcholinesterase assay kit (ab138871, Abcam, UK) according to the manufacturer's instructions. The assay

is based on Ellman's method, in which acetylthiocholine is hydrolyzed by acetylcholinesterase to produce thiocholine, which reacts with 5,5′-dithiobis(2-nitrobenzoic acid) (DTNB) to form a yellow chromophore measured at 410 nm. The kit provides purified acetylcholinesterase standard (5 units per vial), which was reconstituted to obtain a 50 units/mL stock solution. Serial dilutions (0 - 1,000 mU/mL) were prepared to generate a standard curve.

Each well contained 50 µL of sample, standard, or control solution and 50 µL of acetylthiocholine reaction mixture (final volume 100 µL per well) based on **Table 1**. The reaction mixture consisted of assay buffer supplemented with 1X acetylthiocholine substrate and 1X DTNB. Plates were incubated at room temperature for 20 min under protected light conditions, and absorbance increase was monitored continuously at 410 nm to ensure measurements were taken within the linear reaction phase. Donepezil was used as the positive control inhibitor, while solvent-only wells served as negative controls and blanks. IC_{50} values were calculated using nonlinear regression analysis based on concentration-response curves. IC_{50} values of the extract were expressed in µg/mL, whereas reference inhibitor concentrations were additionally converted to µM for comparative discussion.

Table 1 Volume of reagents in AChE inhibitory activity assay.

Reagents	Treatment			
	Blank	**Negative control**	**Positive control**	**Sample**
ddH_2O (µL)	50	50	-	-
Assay buffer (µL)	50	-	-	-
AChE 300 U/mL (µL)	-	50	50	50
ACTh *mix*	50	50	50	50
Donepezil HCl (µL)	-	-	50	-
Sample (µL)	-	-	-	50

Enzyme activity and percentage inhibition are calculated using the following equation:

$$\text{Inhibition (\%)} = \left[\frac{\text{negative control activity} - \text{sample activity}}{\text{negative control activity}}\right] \times 100\% \quad (x)$$

[23]

Molecular docking

Molecular docking analyses were conducted using YASARA Structure (version 19.9.17, licensed to imart@ipb.ac.id YASARA IMBM, University of Graz, Austria). The receptor-inhibitor complex (ChainA.pdb) was initially loaded into YASARA, and a grid box was defined around the native inhibitor binding site. Subsequently, an optimized grid box was generated using the validated grid parameters obtained from the Simulation module. To validate the docking protocol, the co-crystallized ligand (donepezil) was re-docked into the active site of AChE (PDB ID: 6O4W). The crystal structure of human acetylcholinesterase complexed with donepezil (PDB ID: 6O4W) was selected due to its high resolution and the presence of a co-crystallized reference inhibitor, enabling validation of the docking protocol and accurate definition of the active-site grid. The root mean square deviation (RMSD) between the crystallographic pose and the re-docked pose was calculated.

An RMSD value below 2.0 Å was considered acceptable for docking validation. The corresponding simCELL object was automatically generated and displayed in the right-panel table. The prepared system was then saved as a YASARA Scene (.sce) file. The *dock_runscreening* macro was copied into the working directory, and the docking parameters were configured according to the experimental requirements. The receptor scene file (6O4W_receptor.sce) was then opened in YASARA, followed by the import of the ligand dataset. The combined ligand file was separated into individual ligand entries to enable simultaneous docking. The final system configuration was saved as 6O4W.sce. Docking simulations were executed via the Marco & Movie interface to run the *dock_runscreening* macro. Upon completion, YASARA automatically generated output files within the working directory. Each resulting .yob file was subsequently converted into

PDB format for further structural evaluation and post-docking analyses [24,25].

ADMET predictions and drug-likeness properties

The evaluation was performed using the SwissADME website (www.swissadme.ch/) by entering the 2D structure of the compounds. The parameters analyzed refer to Lipinski's Rule of Five, which consists of molecular weight, log P, number of hydrogen bond donors, and acceptors. Furthermore, the physicochemical properties and toxicological aspects of each compound were analyzed through ADMET (Adsorption, Distribution, Metabolism, Excretion, Toxicology) prediction via the pkCSM website (https://biosig.lab.uq.edu.au/pkcsm/). The analysis parameters at this stage consisted of %HIA (Human Intestinal Absorption) values, Caco-2 cell permeability (Cancer coli-2), BBB (Blood-Brain Barrier Penetration) ability, PPB (Plasma Protein Binding), and toxic potential based on Ames tests and carcinogenicity in test animals (Rodent Carcinogenicity) [26].

Data analysis

Statistical methods were used to analyze the impact of *C. xanthorrhiza* rhizome extract on the quantification of secondary metabolites, antioxidant capacity, and acetylcholinesterase inhibition. The analysis was carried out using Minitab 17 software. All experiments were conducted in triplicate (n = 3), and results are expressed as mean ± standard deviation unless otherwise stated. Assumptions of normality and homoscedasticity were verified prior to ANOVA analysis. One-Way ANOVA was applied at a 95% confidence level, with significant differences marked by a p-value < 0.05.

Results and discussion

The results showed that the average moisture content of the 3 replicates of *C. xanthorrhiza* rhizome powder was 4.14%, with the concentrated product appearing brownish yellow. This result is lower than the previous study, which was 7.93% [27]. The percentage obtained meets the low category, in accordance with the standard moisture content requirements set to maintain the quality of the powder, which is < 10%. According to the Pharmacopoeia, low moisture content in powder can extend shelf life and inhibit the decay process [28].

The extraction yield of *C. xanthorrhiza* rhizomes from Sukabumi was 31.61%. This yield value is higher than that found in the previous study, in which the yield of 96% ethanol extract of *C. xanthorrhiza* rhizomes from Takalar, South Sulawesi, Indonesia, using the maceration method was only 12.26% [29]. In addition, research conducted by Widyastuti *et al*. [30] showed a yield percentage of 19% for the methanol extract of *C. xanthorrhiza* from Beringharjo Market, Yogyakarta, Indonesia. The extract results show the effectiveness of the solvent in extracting a compound without showing the capacity level [31].

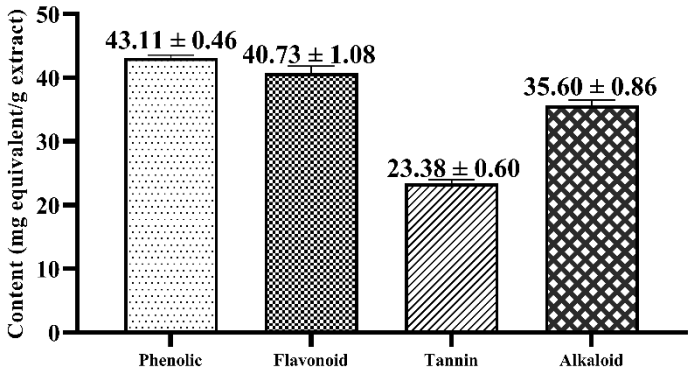

Figure 1 Secondary metabolite content of *Curcuma xanthorrhiza* extract.

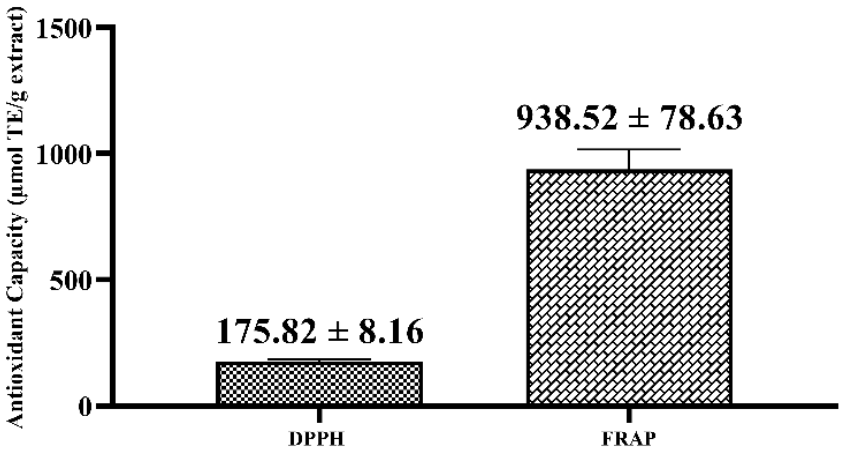

Figure 2 Antioxidant capacity of *Curcuma xanthorrhiza* extract.

The total phenolic content obtained was 43.11 ± 0.46 mg GAE/g extract (**Figure 1**). The results showed that the total phenolic content of *C. xanthorrhiza* rhizomes from Sukabumi, West Java, Indonesia, was different from previous studies. The previous study showed lower results in 80% ethanol extracts from 3 varieties of *C. xanthorrhiza* in 3 different locations. The total phenolic content of the Kursina 1, 2, and 3 (C1, C2 and C3) varieties planted in Bogor, West Java, Indonesia, was 6.780, 7.304, and 7.236 mg GAE/g DW, respectively [32]. The total flavonoid content obtained was 40.73 ± 1.08 mg QE/g extract (**Figure 1**). These results show different total flavonoid contents compared to previous studies. Research conducted by a previous study showed that the total flavonoid content of *C. xanthorrhiza* methanol extract from Johor, Malaysia, using the maceration method was 27.32 ± 7.75 µg QE/mg DW [33]. Research conducted by a previous study showed that the total flavonoid content of *C. xanthorrhiza* methanol extract from Purwodadi, Central Java, Indonesia, using the freeze-dry concentration process was 141.70 ± 8.12 mg QE/g extract [34].

The total tannin content obtained was 23.38 ± 0.60 mg TAE/g extract (**Figure 1**). These results show that the total tannin content of *C. xanthorrhiza* from Sukabumi is higher than in previous studies. Research conducted by a previous study used methanolic extract from *Curcuma caesia* grown on MSB5 medium [35]. The results showed total tannin levels of 2.5 mg TAE/g DW. The previous research also showed lower results, namely 535 mg/100 g in black turmeric extract from Pekanbaru using 70% ethanol solvent [36]. The total alkaloid content obtained was 35.60 ± 0.86 mg CE/g extract (Figure 1). The total alkaloid content obtained showed lower results compared to previous research. The previous research used extracts of rhizomes black turmeric (*C. caesia* Roxb.) from Tamil Nadu, India, with methanol as the solvent. The total alkaloid content obtained 227.34 mg AE/g [37]. The previous research also showed lower results in 70% ethanol extracts from black turmeric rhizomes (*C. caesia* R.) from Pekanbaru, namely 300 mg/100 g [36].

The DPPH antioxidant capacity obtained was 175.82 ± 8.16 µmol TE/g extract (**Figure 2**). The antioxidant capacity results obtained using this method differ from those of previous studies. The previous study showed lower antioxidant capacity in 80% ethanol extracts from 3 varieties of *C. xanthorrhiza* in 3 different locations. The antioxidant capacities of varieties kursina 1, 2, and 3 (C1, C2 and C3) planted in Bogor were 14.64, 14.96, and 12.15 in units of µmol TE/g DW when compared to the Sukabumi (8.53 µmol TE/g DW) and Cianjur (11.72 µmol TE/g DW) regions [32].

Meanwhile, ethanol extracts from 10 accessions of *C. xanthorrhiza* rhizomes from Jambi Province showed relatively low antioxidant capacity, ranging from 0.13 ± 0.02 to 1.11 ± 0.02 µmol TE/g DW [38]. The antioxidant capacity obtained using the FRAP method was 938.52 ± 78.63 µmol TE/g extract (**Figure 2**). The antioxidant capacity results obtained using this method differ from those of previous studies. The previous study reported that the FRAP antioxidant capacity of ethanol extracts of 10 Jambi *C. xanthorrhiza* rhizome accessions had lower power, ranging from 7.71 ± 1.29 to 81.48 ± 4.43

μmol TE/DW [38]. Meanwhile, *C. xanthorrhiza* rhizomes from Bogor with acetone as the solvent showed lower antioxidant capacity, namely 51.24 ± 1.32 (Cursina 1); 115.23 ± 2.30 (Cursina 2) and 82.68 ± 1.50 (Cursina 3) compared to those from Sukabumi [39]. Based on antioxidant capacity data from previous studies, 70% ethanol extracts from *C. xanthorrhiza* rhizomes from Sukabumi have higher antioxidant capacity.

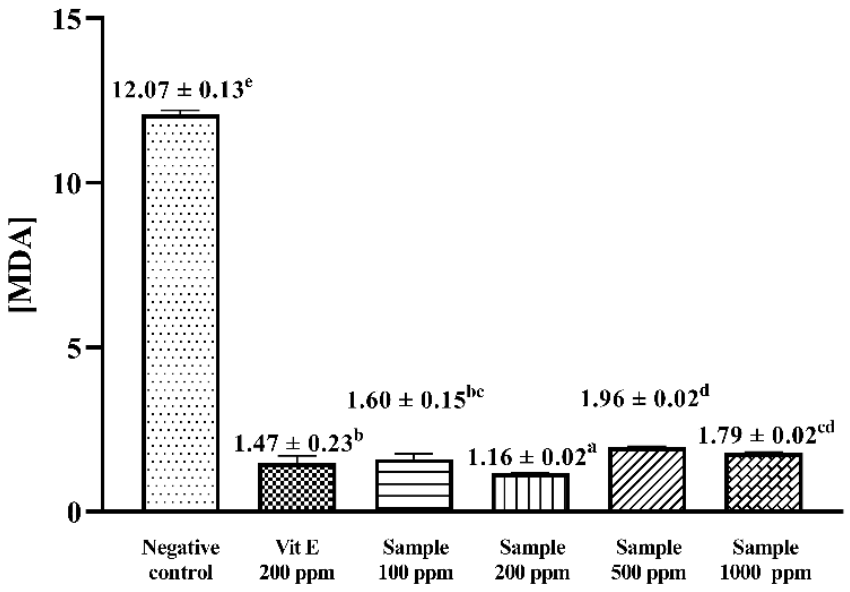

Figure 3 Malondialdehyde levels resulting from lipid peroxidation of various concentration extract and vitamin E.

The maximum linoleic acid incubation time obtained was on day 7. The inhibition of MDA formation was expressed in terms of MDA levels and inhibition percentage. The lowest MDA level formed from the peroxidation process through incubation at 40 °C was 1.16 ± 0.02 (**Figure 3**). The TBA method inhibition percentage obtained was 90.37% with a positive control of vitamin E at 87.86%. The antioxidant results of the extract showed higher results compared to research using *C. aromatica* ethanolic extract samples, which was 85.13 ± 0.23% [40, 41]. Suhendra's study using turmeric extract (*C. domestica* Val.) with varying ethanol solvents (0%, 10%, 30%, 50%, 70% and 90%) showed similar antioxidant activity in inhibiting MDA formation [42]. According to a previous study, the inhibition of MDA formation is likely mediated by the presence of curcuminoid compounds, which belong to the phenolic group, through the mechanism of electron donation to free radical compounds [43].

A comparison of the MDA inhibition capacity of the positive control and extracts at various concentrations (100, 200, 500 and 1,000 mg/L) is presented in **Figure 3**. The comparison shows that the antioxidant capacity of the positive control and extracts differed significantly ($p < 0.05$) in all 4 samples. The inhibition of MDA formation obtained is presented in the form of [MDA] based on the equation value obtained from the TMP standard curve. The lowest MDA concentration was in the 200 mg/L sample extract at 1.16 ± 0.02, while the highest MDA concentration was in the 500 mg/L sample extract at 1.96 ± 0.02. The results of Duncan's multiple range test showed that the inhibition ability of the 4 concentrations had a significant antioxidant effect on linoleic acid peroxidation compared to the untreated condition (negative control).

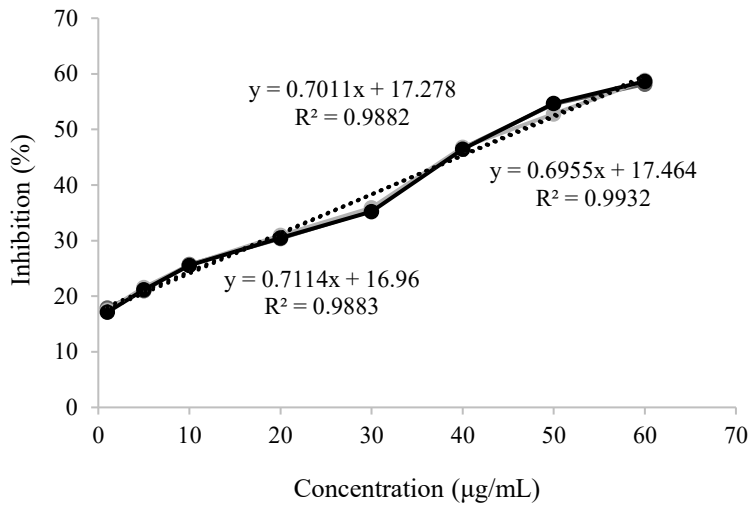

Figure 4 Dose-response curve of *C. xanthorrhiza* ethanolic extract in the acetylcholinesterase inhibition assay.

Table 2 Percentage inhibition of AChE by donepezil and *C. xanthorrhiza.*

Sample	IC_{50} (µg/mL)
Donepezil	0.03 ± 0.00
C. xanthorrhiza	46.63 ± 0.17

The inhibitory activity of C. xanthorrhiza extract against AChE was evaluated at various concentrations (**Figure 4**). The percentage of inhibition increased progressively with increasing extract concentration. This indicates a dose-dependent inhibitory effect on AChE activity. Linear regression analysis shows a strong relationship between concentration and inhibitory activity, as evidenced by a coefficient of determination (R^2) value of 0.9932. The regression equations obtained are y = 0.7114x + 16.96 (R^2 = 0.9883), y = 0.7011x + 17.278 (R^2 = 0.9882), and y = 0.6955x + 17.464.

Donepezil is a commercial drug for Alzheimer's disease, certainly has very strong activity. AChE inhibition activity testing was carried out at a maximum wavelength of 410 nm and an optimum incubation time of 20 min. The data obtained showed that the average IC_{50} value of donepezil was 0.03 µg/mL, as presented in **Table 2**. Donepezil is a compound composed of a benzilpiperidine structure connected to dimethoxy indanone via a methylene group [44]. This drug binds selectively, reversibly, and non-competitively to the peripheral anionic site of AChE [45]. The results of the study showed high inhibitory power against AChE. The IC_{50} value obtained was 0.03 µg/mL, which indicates very strong activity (< 10 µg/mL). *C. xanthorrhiza* extract showed the AChE inhibition test results obtained show potential as an AChE inhibitor agent, with an average IC_{50} value of 46.63 µg/mL. The IC_{50} value of the ethanol extract of *C. xanthorrhiza* AChE indicates a fairly strong inhibitory potential against the AChE enzyme.

The determination of AChE enzyme activity inhibition also uses the commercial anti-Alzheimer's drug donepezil. This drug binds selectively, reversibly, and non-competitively to the peripheral anionic site of AChE [45]. The results presented in **Table 2** show high inhibitory activity against AChE. The IC_{50} value obtained was 0.03 µg/mL or 0.07 µM, indicating very strong activity (< 10 µg/mL). This IC_{50} value is comparable to several previous studies showing donepezil IC_{50} ranging from 0.05 µM (0.02 µg/mL) against electric eel AChE, 0.046 µM (0.02 µg/mL) in the Ellman method AChE assay, to 0.40 µM (0.15 µg/mL) in different enzyme systems and experimental conditions. The differences in IC_{50} values between these studies may be influenced by differences in enzyme sources, substrate concentrations, buffer conditions, and testing parameters used [46-48].

Testing of the inhibition of AChE activity by turmeric rhizome extract showed good potential as an inhibitor with a recorded IC_{50} value of 46.63 µg/mL

(**Table 2**). The IC_{50} value of curcuma rhizome ethanol extract AChE indicates strong inhibitory potential against the AChE enzyme. These results show a lower inhibitory power compared to turmeric extract (*Curcuma longa* L.) with an IC_{50} value of 5.21 µg/mL [49]. Enzyme inhibition activity is categorized into 4 categories based on the IC_{50} value. Very strong activity (< 10 µg/mL), strong activity (10 - 50 µg/mL), moderate activity (50 - 100 µg/mL), and weak activity (> 100 µg/mL) [50]. The active compounds of interest are likely polar compounds that contribute to enzyme inhibition.

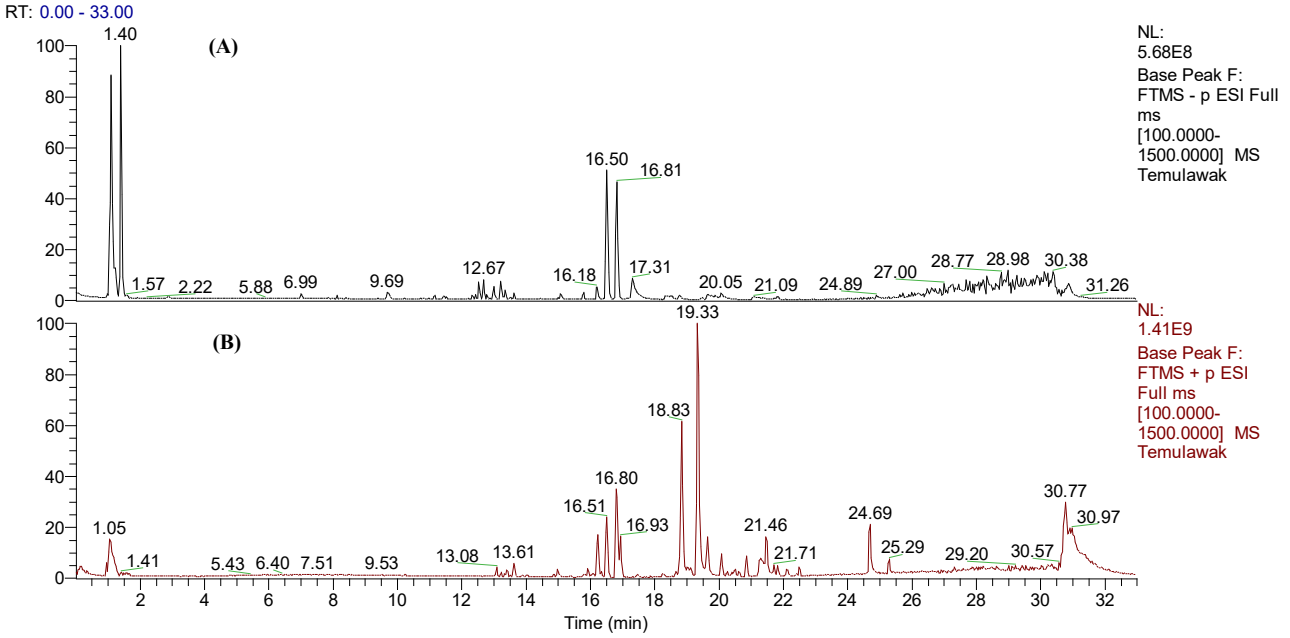

Figure 5 Chromatogram of metabolite profiling extract ethanol *C. xanthorrhiza* results using UHPLC-Q-Orbitrap HRMS; (A) negative ionization and (b) positive ionization.

Table 3 m/z and MS2 metabolites data identified in *C. xanthorrhiza* rhizome extract using UHPLC-Q-Orbitrap-HRMS.

Nu	Metabolite	Formula	Ionization	m/z	MS2	RT	Group
1	*N-acetyl-β-neuraminic acid*	$C_{11}H_{19}NO_9$	$[M+H]^+$	310.11	310, 292, 274, 273	1.057	Saccharide derivatives
2	*Valine*	$C_5H_{11}NO_2$	$[M+H]^+$	118.08	118, 58, 72	1.068	Amino acid
3	*D-glucose*	$C_6H_{12}O_6$	$[M-H]^-$	179.95	59, 71, 79, 89, 101	1.076	Saccharide
4	*Sucrose*	$C_{12}H_{22}O_{11}$	$[M-H]^-$	341.10	71, 89, 101, 179	1.084	Saccharide
5	*Citric acid*	$C_6H_8O_7$	$[M-H]^-$	191.01	111, 87, 85, 191	1.091	Organic acid
6	*Mallic acid*	$C_4H_6O_5$	$[M-H]^-$	133.01	115, 71, 133, 89	1.094	Organic acid
7	*Leucine*	$C_6H_{13}NO_2$	$[M+H]^+$	132.10	86, 69, 56, 132, 97	1.613	Amino acid
8	*Phenylalanine*	$C_9H_{11}NO_2$	$[M+H]^+$	166.08	120, 103, 166	2.482	Amino acid
9	*2-(α-mannopyranosyl)-L-tryptophan*	$C_{17}H_{22}N_2O_7$	$[M+H]^+$	367.14	229, 230, 247	4.680	Amino acid derivative
10	*Tryptophan*	$C_{11}H_{12}N_2O_2$	$[M+H]^+$	205.09	188, 205, 170, 143	5.097	Amino acid
11	*Zedoarofuran*	$C_{15}H_{20}O_4$	$[M+H]^+$	265.14	229, 247, 265	11.235	Sesquiterpen
12	*Curcumenolactone A*	$C_{15}H_{20}O_3$	$[M+H]^+$	249.14	249, 203, 143, 105	12.804	Sesquiterpen

Nu	Metabolite	Formula	Ionization	m/z	MS2	RT	Group
13	*Cyclocurcumin*	$C_{21}H_{20}O_6$	$[M+H]^+$	369.13	175, 160, 135	13.209	Polyphenol
14	*Curcumenolactone C*	$C_{15}H_{20}O_4$	$[M+H]^+$	265.14	201, 229, 247, 265	13.348	Sesquiterpen
15	*Curcumadione*	$C_{15}H_{22}O_2$	$[M+H]^+$	235.16	93, 95, 105	13.411	Sesquiterpen
16	*Zedoarol*	$C_{15}H_{18}O_3$	$[M+H]^+$	247.13	247, 229, 189	13.585	Sesquiterpen
17	*Zederone*	$C_{15}H_{18}O_3$	$[M+H]^+$	247.13	247, 229, 183	13.872	Sesquiterpen
18	*13-Hydroxygermacrone*	$C_{15}H_{22}O_2$	$[M+H]^+$	235.16	235, 217, 199	14.984	Sesquiterpen
19	*Curcumenol*	$C_{15}H_{22}O_2$	$[M+H]^+$	235.16	235, 217	15.412	Sesquiterpen
20	*(6s)-6-methyl-5-(3-oxobutyl)-2-(propan-2-ylidene)-cyclohept-4-en-1-one*	$C_{15}H_{22}O_2$	$[M+H]^+$	235.16	175, 147, 133	15.921	Sesquiterpen
21	*Bisdemethoxycurcumin*	$C_{19}H_{16}O_4$	$[M-H]^-$	307.09	119, 143, 187, 145, 307	16.201	Polyphenol
22	*Dehydrocurdione*	$C_{15}H_{22}O_2$	$[M+H]^+$	235.16	161, 135, 119, 107, 105, 93, 83	16.223	Sesquiterpen
23	*Sophoraflavanone B*	$C_{20}H_{20}O_5$	$[M-H]^-$	339.12	119, 219, 339	16.225	Flavonoid
24	*Furanodiene*	$C_{15}H_{20}O$	$[M+H]^+$	217.15	161, 217, 119, 157	16.241	Sesquiterpen
25	*Demethoxycurcumin*	$C_{20}H_{18}O_5$	$[M-H]^-$	337.10	147, 177, 145, 119, 117, 149	16.500	Polyphenol
26	*Curcumin*	$C_{21}H_{20}O_6$	$[M+H]^+$	369.13	177, 145, 285, 117, 369	16.804	Polyphenol
27	*Bisphenol A*	$C_{15}H_{16}O_2$	$[M+H]^+$	229.12	229, 201, 159, 95, 109	16.933	Polyphenol
28	*Tetradecylamine*	$C_{14}H_{31}N$	$[M+H]^+$	214.25	214, 85, 71	18.468	Amine
39	*Iso-velleral*	$C_{15}H_{20}O_2$	$[M+H]^+$	233.15	233, 215, 173, 187	18.710	Sesquiterpen
30	*Turmeronol A*	$C_{15}H_{20}O_2$	$[M+H]^+$	233.15	83, 135, 91, 150	18.710	Sesquiterpen
31	*Cinnamic acid*	$C_9H_8O_2$	$[M+H]^+$	149.05	149, 103	18.829	Organic acid
32	*Pyrocurzerenone*	$C_{15}H_{16}O_2$	$[M+H]^+$	213.12	213, 198, 128	18.831	Sesquiterpen
33	*(+)-Germacrone-4,5-epoxide*	$C_{15}H_{22}O_2$	$[M+H]^+$	235.16	119, 131	19.029	Sesquiterpen
34	*Safrole*	$C_{10}H_{10}O_2$	$[M+H]^+$	163.07	163, 105, 91, 79	19.333	Phenylpropene
35	*Isosafrole*	$C_{10}H_{10}O_2$	$[M+H]^+$	163.07	135, 117, 107, 123	19.333	Phenylpropene
36	*Curzerenone*	$C_{15}H_{18}O_2$	$[M+H]^+$	231.13	231, 203, 213, 185, 149	19.637	Sesquiterpen
37	*Curcumene*	$C_{15}H_{22}$	$[M+H]^+$	203.17	203, 147, 119, 91	20.076	Sesquiterpen
38	*Ar-turmerone*	$C_{15}H_{20}O$	$[M+H]^+$	217.15	119, 120, 117, 91, 67, 109	20.845	Sesquiterpen
39	*α-methylstyrene*	C_9H_{10}	$[M+H]^+$	119.08	117, 115, 103	20.847	Aromatic
40	*Heptylbenzene*	$C_{13}H_{20}$	$[M+H]^+$	177.16	177, 175	21.433	Aromatic
41	*Xanthorrhizol*	$C_{15}H_{22}O$	$[M+H]^+$	219.17	219, 69, 201, 145, 159	21.459	Sesquiterpen
42	*Elixene*	$C_{15}H_{24}$	$[M+H]^+$	205.19	121, 93, 107, 105	21.701	Sesquiterpen
43	*Elemene*	$C_{15}H_{24}$	$[M+H]^+$	205.19	121, 149, 81	21.865	Sesquiterpen

Metabolite profiling results of *C. xanthorrhiza* rhizome extract using the same instrument with positive ESI $[M+H]^+$ and negative [M-H]- showed 43 compounds detected in **Figure 5** and **Table 3**. Of the total 43 compounds identified, there were flavonoids, curcuminoids, sesquiterpenes, and other organic compounds. On the other hand, 22 of these compounds were sesquiterpenes that were successfully identified as xanthorrhizol, curcumenolactone A, zedoarol, curcumenolactone C, ar-turmerone, and so on. The results of this study are in line with previous research in terms of the dominance of terpenoids and curcuminoids identified using UHPLC-Q-Orbitrap-HRMS. However, this research successfully identified a greater number of compounds, namely 43 compounds compared to the 39 metabolites reported by the previous study [51]. The presence of sesquiterpene compounds is highly relevant to the very high terpenoid content in *C. xanthorrhiza* extract. Bisphenol A was excluded from biological interpretation due to its common occurrence as laboratory contaminant. Compound identification was based on accurate mass measurement (mass error < 5 ppm), isotopic pattern analysis, and MS/MS fragmentation matching with reference spectra from databases (PubChem and literature). Identification confidence was assigned according to MSI level 2 (putatively annotated compounds).

The metabolite profile of 70% ethanol extract of *C. xanthorrhiza* rhizome obtained by positive and negative ionization modes in this study is consistent with previous studies. The previous research, which used LC-HRMS + PCA/PLS-DA, focused only on the distinguishing metabolite, namely curcuminoids (curcumin II) and (-)-Caryophyllene oxide, without information on fragmentation and minor metabolites due to the limitations of non-MS detectors [52]. Meanwhile, several previous research studies demonstrated the advantages of HRMS detectors, which enable the identification of a wider range of metabolites, including sesquiterpenes, flavonoids, and polar compounds. The use of HPLC with efficient separation combined with high-resolution orbitrap allows for broader and more specific identification of extract compounds [29,53]. Compounds identified in the extract, such as curcuminoids and sesquiterpenes, have been reported to have neuroprotective activity through antioxidant, anti-inflammatory, and neurotoxic protein aggregation inhibition mechanisms, as well as protection against oxidative stress-induced neuronal damage, which is thought to contribute to the activity of the extract in this study [54-56].

Table 4 Molecular docking results of the best candidate ligands.

Ligand	Groups	Binding Energy (kcal/mol)	Interaction of Ligands with the Essential Amino Acid AChE
Bisdemethoxycurcumin (BDMC)	Curcuminoid	−11.55	**Asp74** **Trp86** Gly120 **Gly121** **Tyr124** **Tyr133** Glu202 **Ser203** **Trp286** Leu289 Ser293 Val294 **Phe295** Arg296 **Phe297** **Tyr337** **Phe338** **Tyr341** **His447** Gly448 Ile451
Cyclocurcumin (CYC)	Curcuminoid	−11.45	**Tyr72** **Asp74** **Trp86** Asn87 Gly120 **Gly121** **Gly122** **Tyr124** **Ser125** Gly126 Leu130 **Tyr133** **Ser203** **Ala204** **Trp286** Val294 **Phe295** Arg296 **Phe297** **Phe338** **Tyr341** **His447**
Donepezil (DPZL)	AChE Inhibitor	−11.34	**Tyr72** **Asp74** **Trp86** Gly120 **Gly121** **Tyr124** **Tyr133** Glu202 **Ser203** **Trp286** Leu289 Ser293 Val294 **Phe295** Arg296 **Phe297** **Tyr337** **Phe338** **Tyr341** **His447** Gly448 Ile451

Ligand	Groups	Binding Energy (kcal/mol)	Interaction of Ligands with the Essential Amino Acid AChE
Demethoxycurcumin (DMC)	Curcuminoid	−11.29	**Asp74** **Trp86** Tyr119 Gly120 **Gly121** **Tyr124** **Ser125** Gly126 Ala127 Leu130 **Tyr133** Glu202 **Ser203** **Trp286** Leu289 Ser293 Val294 **Phe295** Arg296 **Phe297** **Tyr337** **Phe338** **Tyr341** **His447** Gly448 Ile451
Curcumin (CUR)	Curcuminoid	−11.23	**Asp74** **Trp86** Tyr119 Gly120 **Gly121** **Tyr124** **Ser125** Gly126 Ala127 Leu130 **Tyr133** Glu202 **Ser203** **Trp286** Leu289 Ser293 Val294 **Phe295** Arg296 **Phe297** **Tyr337** **Phe338** **Tyr341** **His447** Gly448 Ile451
Xanthorrhizol (XNT)	Sesquiterpen	−8.63	**Asp74** **Trp86** Gly120 **Gly121** Tyr124 **Ser125** Gly126 **Tyr133** **Trp286** **Phe295** **Phe297** **Tyr337** **Phe338** **Tyr341** **His447**

Description: **Blue**: Catalytic Triad; **Purple**: Acyl pocket; **Green**: Catalytic Active Site (CAS); **Red**: Oxyanion hole; **Orange**: Peripheral Anionic Site (PAS)

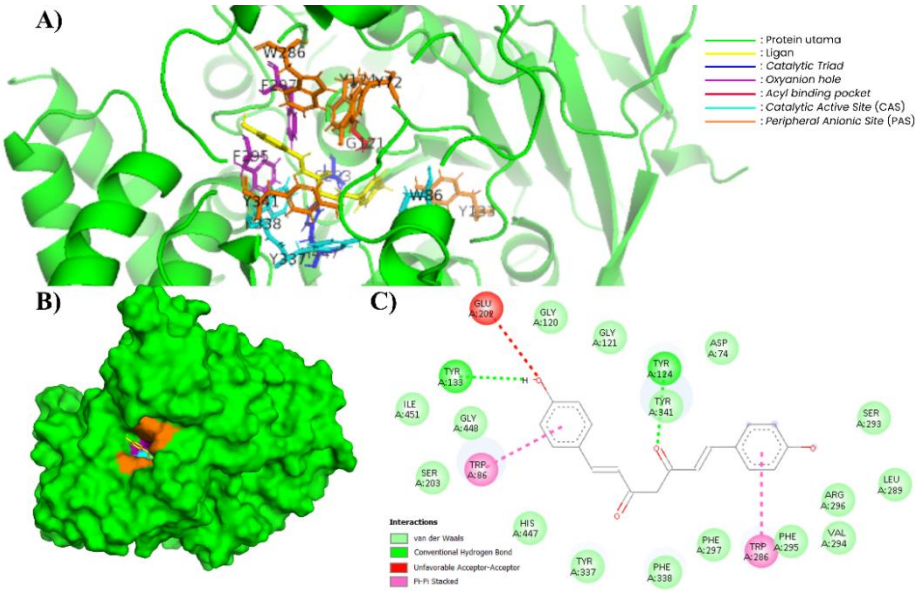

Figure 6 Complex of BDMC and AChE (604W). (A) In the 3-dimensional visualization of BDMC interactions with essential amino acids (PyMOL). (B) BDMC docking in the substrate binding pockets (PyMOL). (C) In the 2-dimensional visualization of BDMC interaction with essential amino acids and polar contact (Discovery Studio).

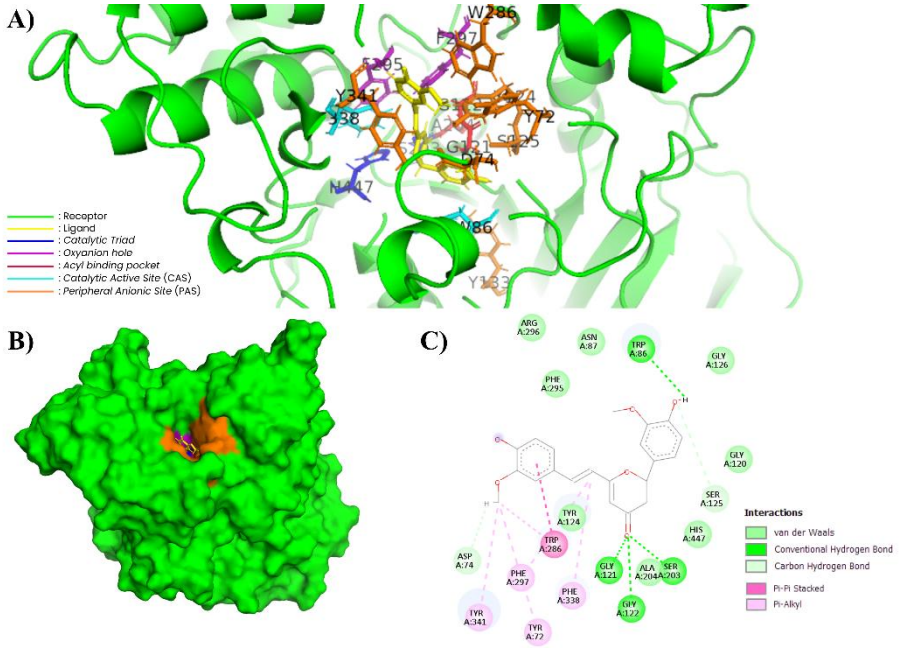

Figure 7 Complex of CYC and AChE (604W). (A) In the 3-dimensional visualization of CYC interactions with essential amino acids (PyMOL). (B) CYC docking in the substrate binding pockets (PyMOL). (C) In the 2-dimensional visualization of CYC interaction with essential amino acids and polar contact (Discovery Studio).

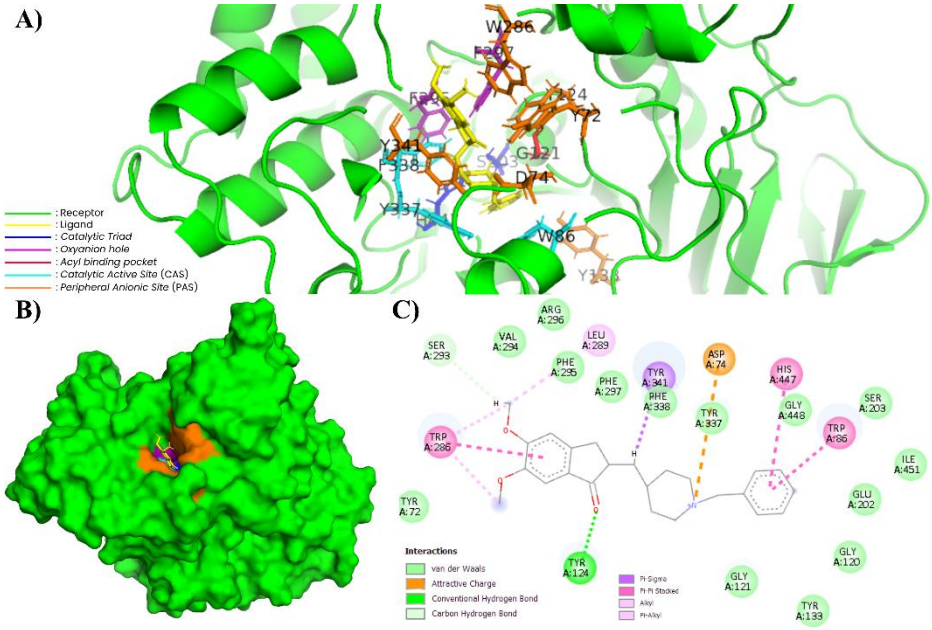

Figure 8 Complex of DPZL and AChE (604W). (A) In the 3-dimensional visualization of DPZL interactions with essential amino acids (PyMOL). (B) DPZL docking in the substrate binding pockets (PyMOL). (C) In the 2-dimensional visualization of DPZL interaction with essential amino acids and polar contact (Discovery Studio).

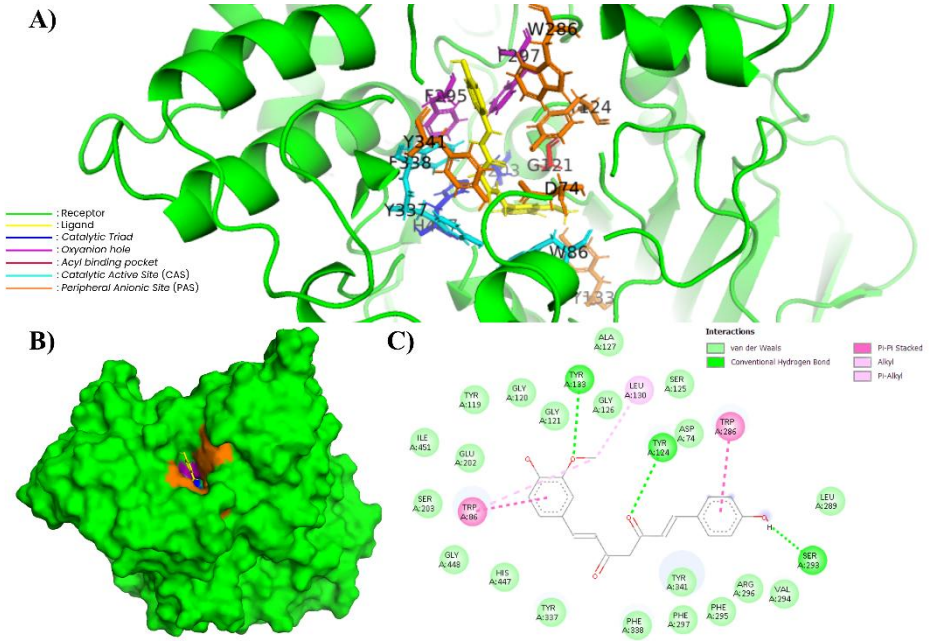

Figure 9 Complex of DMC and AChE (604W). (A) In the 3-dimensional visualization of DMC interactions with essential amino acids (PyMol). (B) DMC docking in the substrate binding pockets (PyMol). (C) In the 2-dimensional visualization of DMC interaction with essential amino acids and polar contact (Discovery Studio).

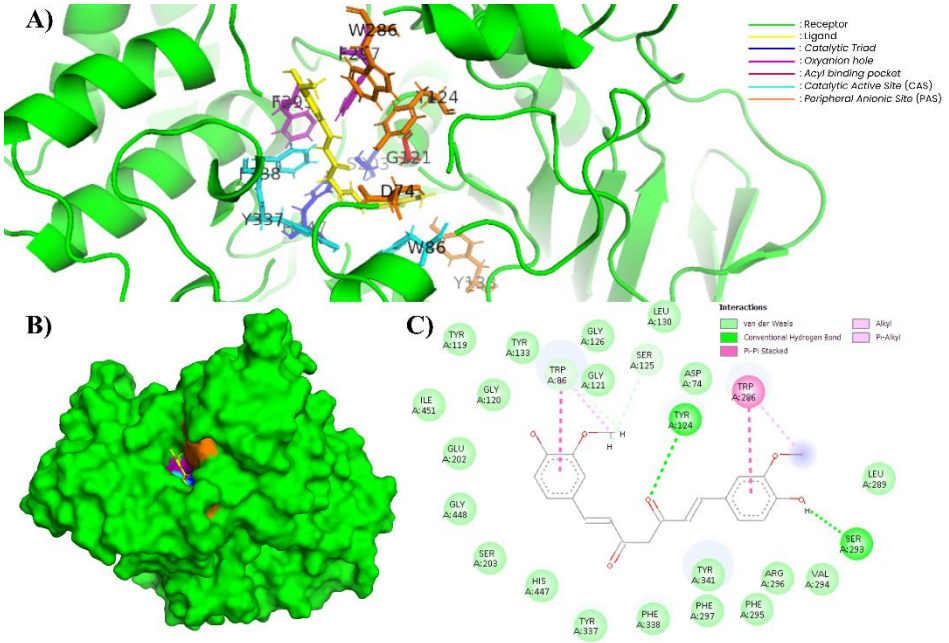

Figure 10 Complex of CUR and AChE (604W). (A) In the 3-dimensional visualization of CUR interactions with essential amino acids (PyMOL). (B) CUR docking in the substrate binding pockets (PyMOL). (C) In the 2-dimensional visualization of CUR interaction with essential amino acids and polar contact (Discovery Studio).

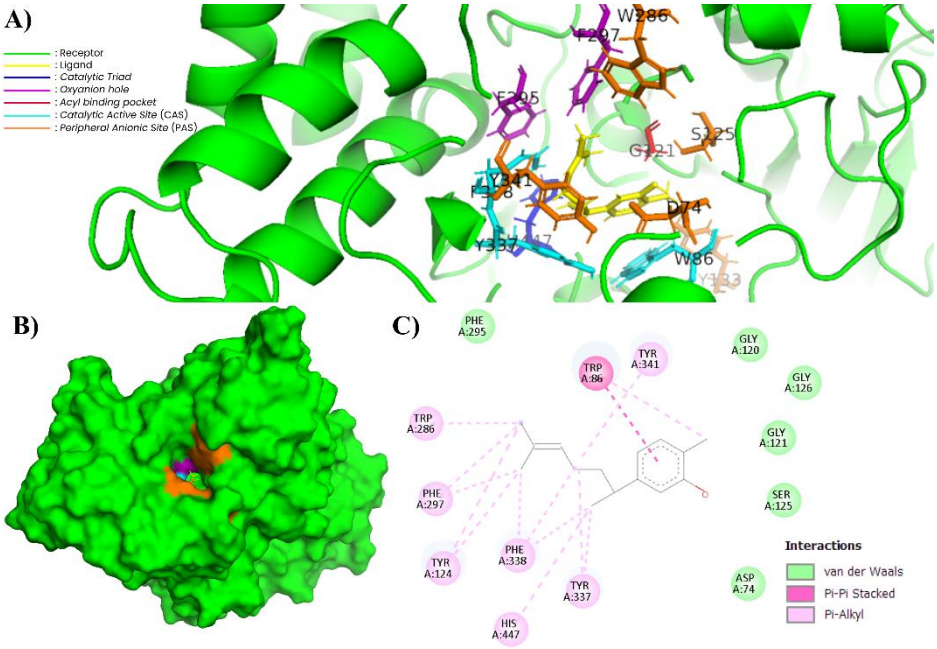

Figure 11 Complex of XNT and AChE (604W). (A) In the 3-dimensional visualization of XNT interactions with essential amino acids (PyMOL). (B) XNT docking in the substrate binding pockets (PyMOL). (C) In the 2-dimensional visualization of XNT interaction with essential amino acids and polar contact (Discovery Studio).

Molecular docking aims to evaluate the interaction between ligands and enzymes based on computation [57]. This simulation is very important and crucial in drug design in pharmaceutical companies [58]. The redocking procedure yielded an RMSD value of 0.001 Å, indicating reliable reproduction of the experimental binding pose and validating the docking protocol. The molecular docking simulation results presented in **Table 4** show that the single compound with the highest binding energy (ΔG) is bisdemethoxycurcumin (BDMC) with a value of −11.55 kcal/mol. The next lowest values in sequence are cyclocurcumin (CYC), donepezil (DPZL), demethoxycurcumin (DMC), curcumin (CUR), and xanthorrhizol (XNT). These compounds were identified from ethanol extracts using LC-MS/MS. In addition, donepezil, a commercial drug for Alzheimer's disease, was used as a positive control. The lowest ΔG value indicates the formation of a bond between the ligand and the receptor [59].

BDMC has a higher binding energy, even exceeding donepezil as a standard AChE inhibitor. This compound interacts with important residues in the peripheral anionic site (PAS) such as Asp74, Tyr124, and Trp286, which play a role in ligand recognition and initial binding [60]. In addition, BDMC also interacts with residues Ser203 and His447, which are part of the catalytic triad in the catalytic active site (CAS). Other interactions are also seen with acyl pocket residues such as Tyr133, Tyr337, and Phe338, as well as oxyanion hole residues Gly120 and Gly121, which function in the stability of reaction intermediates [61]. The 2D and 3D visualizations in Figures 6A and 6B show that BDMC forms hydrogen bonds with Tyr123 and Ser293 and has π–π interactions with Trp86 and Trp286. These interaction results are consistent with the literature, which states that potential AChE inhibitors can interact with PAS and CAS simultaneously, thereby increasing the stability of the ligand-receptor complex [62].

CYC shows a high bond energy of −11.45 kcal/mol and exhibits a fairly broad pattern of residue interactions. The molecular docking results show interactions with important residues in PAS (Tyr72, Asp74 and Trp286). In addition, CYC also forms interactions with the catalytic triad (Ser203 and His447) and surrounding residues such as Trp86 and Ser125. Interactions with the Gly121 and Gly122 residues in the oxyanion hole indicate the formation of hydrogen bonds, while in the acyl pocket (Phe297, Tyr341, Phe338 and Tyr72) there are hydrophobic interactions in the form of π–alkyl. The 2D and 3D visualizations in Figures 7A and 7C show a combination of hydrogen bonds and aromatic interactions that mediate CYC to

bind stably to several functional sites of AChE, which are important characteristics related to the affinity of compounds with AChE [63].

DPZL as a commercial drug and positive control showed a bond energy of -11.34 kcal/mol, characterized by a broad interaction pattern with AChE. Molecular docking results show that DPZL interacts with PAS residues (Trp286 and Ty124), catalytic triad residues (Ser203 and His447), and CAS residues (Trp86). The results also show hydrophobic interactions with residues in the acyl pocket (Try337, Phe338, Leu289 and Tyr341). The 2D and 3D visualizations in Figures 8A and 8C show that DPZL forms hydrogen bonds with Tyr124, π–π interactions with Trp286, Trp86, and Ser293, π–alkyl interactions with Leu289, and π–σ interactions with Tyr341. This interaction pattern strongly represents the stable and multipoint binding mechanism of DPZL at several important sites of AChE, where the indanone group plays a role in hydrophobic interactions and π–π stacking at the PAS, while the piperidine and benzyl rings play a role in interactions around the CAS and catalytic triad [63,64].

DMC and CUR exhibit binding energies of −11.29 and −11.23 kcal/mol, respectively. The interaction patterns of these 2 compounds are nearly identical, involving residues Asp74, Trp86, Gly120, Gly121, Tyr123, Ser203, Trp286, and His447. The involvement of these residues in curcumin and its derivatives indicates that both compounds are stable within the active gorge of AChE, including PAS, CAS, and the oxyanion hole [65]. The 2D visualization in **Figures 9(C)** and **10(C)** shows that both compounds form hydrogen bonds with residues Asp74, Ser203, Gly120, and Gly121, as well as π–π stacking interactions with Trp86 and Trp286. Additionally, π–alkyl and van der Waals hydrophobic interactions involve residues in the acyl pocket (Tyr133, Tyr337, Phe338, and Tyr341). The 3D visualization in Figures 8A and 9A confirms the presence of a planar aromatic framework in both compounds, enabling simultaneous interactions with CAS and PAS. This pattern is consistent with the previous research, that hydrophobic interactions and hydrogen bonds around PAS and CAS produce enzyme-ligand complexes with high stability [66]. In addition, curcumin and its derivatives tend to occupy the aromatic gorge of AChE with moderate to high affinity [67,68].

XNT, which belongs to the sesquiterpene group, shows a relatively lower binding energy of −8.63 kcal/mol. XNT shows interactions with CAS, PAS, and acyl pocket residues. The 2D visualization in **Figure 11(C)** shows that XNT forms π–π stacking interactions with Trp86 and π–alkyl interactions with Tyr341, Tyr337, Phe338, His447, Tyr124, Phe297, and Trp286, which are predominantly hydrophobic in nature. The 3D visualization in **Figure 10(A)** confirms that XNT occupies the active site area, which is dominated by hydrophobic residues. This interaction pattern is consistent with the characteristics of simple hydrocarbon sesquiterpenes that are low in heteroatoms. Previous study stated that simple sesquiterpenes have limited polar functional groups to form strong hydrogen bonds with the catalytic triad of AChE (Ser203 and His447) [69]. The inhibitory activity of terpenoids on AChE is greatly influenced by the presence of oxygen-containing functional groups such as hydroxyl, carbonyl, and lactone, which enable the formation of hydrogen bonds with important residues at the enzyme's active site, thereby increasing the stability of the ligand-enzyme complex. Conversely, simple terpenoids with minimal heteroatoms generally interact only through hydrophobic and π–π forces, contributing to lower AChE inhibitory activity [70-72].

Although the IC_{50} value of the crude extract (46.63 μg/mL) reflects moderate-to-strong inhibition at the extract level, the docking results suggest that this activity likely arises from the combined contribution of curcuminoids and sesquiterpenes. The relatively high binding affinities of BDMC, DMC, and CUR indicate that curcuminoids may contribute to catalytic-site interactions, whereas xanthorrhizol may enhance activity through hydrophobic stabilization within the aromatic gorge. This multi-compound synergy may explain the extract-level inhibition observed *in vitro*.

Table 5 Drug-likeness prediction of the best candidate ligands using SwissADME.

Ligand	Parameter						
	MW (Da)	**H-bond acceptors**	**H-bond donors**	**TPSA (Å^2)**	**GI absorption**	**Lipinski; violations**	**BBB-permeant**
Bisdemethoxycurcumin	308.33	4	2	74.60	High	0	Yes
Cyclocurcumin	368.38	6	2	85.22	High	0	No
Demethoxycurcumin	338.35	5	2	83.83	High	0	No
Curcumin	368.38	6	2	93.06	High	0	No
Donepezil	379.49	4	0	38.77	High	0	Yes
Xanthorrhizol	218.33	1	1	20.23	High	0	Yes

Table 6 Results of pharmacokinetic profile using pkCSM.

Parameter		Ligand					
		BDMC	**CYC**	**DMC**	**CUR**	**DPZL**	**XNT**
Absorption	HIA (%)	91.16	81.35	91.39	82.19	93.71	90.44
	Caco-2 (nm/s)	0.96	1.65	1.02	−0.09	1.27	1.63
Distribution	PPB (%)	95.5	61.8	100	100	100	95.5
	BBB (log BB)	−0.09	−0.24	−0.34	−0.56	0.15	0.42
Metabolism	Substrat CYP34A	✓	-	✓	✓	✓	✓
	Inhibitor CYP34A	✓	-	✓	✓	✓	-
Excretion	Total *clearance* (log mL/min/kg)	−0.01	6.30	0.03	−0.002	0.99	1.22
	LD_{50} oral (mol/kg)	2.09	2.48	1.97	1.83	2.75	2.18
Toxicity	Mutagenicity	-	✓	-	-	-	-
	Hepatotoxicity	-	-	-	-	✓	-

The evaluation of the best ligand candidates pays close attention to pharmacokinetic profiles that are close to commercial drugs with higher safety, in which potency, selectivity, and ADMET parameters are crucial aspects [73,91]. SwissADME analysis shows that all ligands comply with Lipinski's rules without violation, indicating good drug-likeness characteristics. Xanthorrhizol has the lowest molecular weight of 218.33 Da with 1 hydrogen bond donor and 1 hydrogen bond acceptor, while curcuminoids range from 308 - 368 Da [74]. The high compliance with these rules is consistent with the report by previous research, which states a strong relationship between compliance and oral bioavailability [75]. Absorption parameters also show that all ligands have high gastrointestinal absorption capacity, which is influenced by TPSA values ranging from 20.23 to 93.06 Å^2. Lower TPSA values indicate better membrane permeability [76,77].

SwissADME predictions of blood-brain barrier (BBB) permeability using the Boiled-egg model show that donepezil, as a commercial drug, has strong penetration ability, while 2 candidates, bisdemethoxycurcumin and xanthorrhizol, are also included in the yolk area and thus have the potential to reach the central nervous system (**Table 5**) [78,79]. Conversely, curcumin, demethoxycurcumin, and cyclocurcumin are outside the permeable area, consistent with the report by a previous study regarding the limitations of classical curcuminoids in penetrating the BBB [80]. This pattern is in line with pkCSM results,

where positive logBB values for donepezil (0.15) and xanthorrhizol (0.42) confirm their ability to penetrate the BBB, while curcuminoids show negative logBB values, indicating their limited ability to reach the central nervous system [81,82].

Comparison of the 2 sites also shows consistency in absorption and distribution parameters. In SwissADME (**Table 6**), all compounds showed high potential for gastrointestinal absorption, while pkCSM validated these results through high HIA values (> 80%) for all ligands, including donepezil (93.71%) and bisdemethoxycurcumin (91.16%) [69,81]. The Caco-2 permeability parameters from pkCSM reinforce the SwissADME results regarding solubility and permeability, where curcumin shows a very low value (−0.93 nm/s) consistent with its reported poor bioavailability [83]. Additionally, pkCSM distribution predictions indicate that the majority of ligands have PPB > 90%, consistent with the pharmacokinetic properties of donepezil, which is ± 93% bound to plasma proteins [84]. High PPB values indicate a long half-life but low free fraction [59,85].

The pkCSM results provide additional information such as predictions of ligand metabolism, excretion, and toxicity. Metabolism predictions identify curcumin derivatives, except cyclocurcumin, as both substrates and inhibitors of CYP3A4, while xanthorrhizol is only a substrate, resulting in a lower risk of metabolic interactions [86,87]. Excretion parameters indicate that xanthorrhizol and donepezil have a total clearance > 1 log mL/min/kg, indicating rapid elimination of the compound and a low risk of accumulation [88-90]. pkCSM toxicity analysis shows that only cyclocurcumin is mutagenic and donepezil is predicted to be hepatotoxic, consistent with clinical reports [87]. The integration of SwissADME and pkCSM shows that xanthorrhizol meets the pharmacokinetic requirements as the most promising candidate [92]. Although docking and ADMET analyses suggest potential activity, experimental validation of isolated compounds, particularly xanthorrhizol, is required to confirm AChE inhibition at the molecular level.

Conclusions

The ethanol extract of *C. xanthorrhiza* rhizome exhibits high secondary metabolite content, strong antioxidant capacity, significant lipid peroxidation activity, and AChE inhibition ability with a relatively strong IC_{50} value. Although oxidative stress is implicated in Alzheimer's pathology, this study does not experimentally demonstrate a direct mechanistic link between antioxidant activity and AChE inhibition. Metabolite profiling results show that the ethanol extract of *C. xanthorrhiza* rhizome contains dominant compounds belonging to the curcuminoid and sesquiterpene groups. The identified active compounds, namely bisdemethoxycurcumin (BDMC), cyclocurcumin (CYC), demethoxycurcumin (DMC), curcumin (CUR), and xanthorrizol (XNT), showed potential as AChE inhibitors based on *in silico* analysis. Among these compounds, XNT (xanthorrhizol) shows the most promising potential because it has stable and sufficiently strong interactions with AChE, accompanied by a favorable pharmacokinetic profile, good bioavailability and bioactivity, and low oral toxicity. Although the findings are limited to *in vitro* and *in silico* analyses, the integrated metabolomics–bioactivity-ADMET approach employed in this study provides a rational framework for prioritizing natural compounds as potential AChE inhibitors. Further *in vivo* validation and blood-brain barrier permeability studies are required to confirm the therapeutic relevance of xanthorrhizol and related compounds.

Acknowledgements

The authors thank the Reguler Fundamental Research for funding this research by contract No. 2342/IT3.D10/PT.01.03/P/B/2025.

Declaration of generative AI in scientific writing

The authors confirm that generative AI tools, including DeepL and OpenAI's ChatGPT, were utilized solely for language refinement and grammatical editing during the preparation of this manuscript. These tools were not employed to generate any content or to analyze or interpret data. The authors assume full responsibility for the accuracy and conclusions presented in this manuscript.

CRediT author statement

Faishal Ahmad Arbi: Conceptualization, Methodology, Data curation, Software, Formal analysis, Investigation, Validation, Visualization, and Writing – Drafting of original manuscript. **Dimas Andrianto:**

Conceptualization, Methodology, Data curation, Formal analysis, Investigation, Validation, and Writing – Review & Editing manuscript. **Dewi Anggraini Septaningsih:** Conceptualization, Methodology, Supervision, Validation, and Writing – Review & Editing manuscript. **Ukhradiya Magharaniq Safira Purwanto:** Methodology, Data curation, Investigation, Validation, and Writing – Review & Editing manuscript. **Rini Kurniasih:** Methodology, Validation, Supervision, and Writing – Review & Editing manuscript. **Mega Safithri:** Conceptualization, Methodology, Supervision, Project administration, Funding acquisition, Validation, Fundraising, and Writing – Review & Editing manuscript.

References

[1] G Livingston, J Huntley, KY Liu, SG Costafreda, G Selbæk, S Alladi, D Ames, S Banerjee, A Burns, C Brayne, NC Fox, CP Ferri, LN Gitlin, R Howard, HC Kales, M Kivimäki, EB Larson, N Nakasujja, K Rockwood, Q Samus and N Mukadam. Dementia prevention, intervention, and care: 2024 report of the *Lancet* standing commission. *The Lancet* 2024; **404(10452)**, 572-628.

[2] A Houldsworth. Role of oxidative stress in neurodegenerative disorders: A review of reactive oxygen species and prevention by antioxidants. *Brain Communications* 2024, **6(1)**, fcad356.

[3] World Health Organization. *Global dementia observatory dementia.* World Health Organization, 2022.

[4] YTA Reubun, S Kumala, S Setyahadi and P Simanjuntak. Inhibition of acetylcholinesterase by extracts of gotu kola (*Centella asiatica* (L.) Urb), moringa (*Moringa oleifera* Lam.) leaves and their combinations. *PHARMACY: Jurnal Farmasi Indonesia* 2021; **17(2)**, 451-458.

[5] F Az-Zahra, J Afidika, SDA Diamantha, AE Rahmani, S Fatimah, DL Aulifa, AA Elaine and BDP Sitinjak. *In silico* study of betel leaves compound (*Piper betle* L.) as acetylcholinesterase (AChE) enzyme inhibitor in Alzheimer disease. *Indonesia Journal of Biological Pharmacy* 2022; **2(2)**, 44-58.

[6] N Bittner, CSM Funk, A Schmidt, F Bermpohl, EJ Brandl, EEA Algharably, R Kreutz and TG Riemer. Psychiatric adverse events of acetylcholinesterase inhibitors in Alzheimer's disease and Parkinson's dementia: Systematic review and meta-analysis. *Drugs & Aging* 2023; **40**, 953-964.

[7] Y Harun, Y Diansari, S Marisdina and Y Felistia. Effectivity of donepezil in cognitive function of postoperative intracranial tumour patients. *Neurona* 2020; **37(2)**, 143-151.

[8] M Safithri, EB Koendhori, D Andrianto, R Kurniasih, MA Dwicesaria, EYY Nurinsani, MA Umar and M Hufdayanti. Analysis of bioactive compounds *Piper crocatum* as inhibitors of acetylcholinesterase *in silico* and *in vitro*. *Trends in Sciences* 2025; **22(4)**, 9437.

[9] N Jusril, ANN Muhamad Juhari, SI Abu Bakar, WM Md Saad and MI Adenan. Combining *in silico* and *in vitro* studies to evaluate the acetylcholinesterase inhibitory profile of different accessions and biomarker triterpenes of *Centella asiatica*. *Molecules* 2020; **25(15)**, 3353.

[10] MA Khairinisa, TM Fakih and DSF Ramadhan. Bioactive potential of *Centella asiatica* leaf extract in acetylcholinesterase inhibition: Insights from multiple ligand mapping. *Computers in Biology and Medicine* 2025; **197(A)**, 110970.

[11] MAS Kurniawan, MJ Baari, Sariyanti and Finarisnawati. QSAR analysis using semi-empirical AM1 method, molecular docking, and ADMET studies of chalcone derivatives as antimalarial compounds. *Jurnal Kimia Riset* 2023; **8(2)**, 186-199.

[12] W Nurcholis, R, Alfadzrin, N Izzati, R Arinati, BÁ Vinnai, F Sabri, E Kristof and MI Artika. Effects of methods and durations of extraction on total flavonoid and phenolic contents and antioxidant activity of Java cardamom (*Amomum compactum* Soland Ex Maton) fruit. *Plants* 2022. **11(17)**, 2221.

[13] M Safithri, S Indariani and D Septiyani. Antioxidant activity and total phenolic content of functional beverages nanoencapsulation based on red betel extract. *Indonesian Journal of Human Nutrition* 2020; **7(1)**, 69-83.

[14] TB Yuniasih, M Safithri and Syaefudin. *In vitro* analysis of gradual water extract of red betel lead (*Piper crocatum*) as free radical scavenging and inhibitor of α-glucosidase. *Current Biochemistry* 2023; **10(1)**, 38-45.

[15] W Nurcholis, R, Alfadzrin, N Izzati, R Arinati, BÁ Vinnai, F Sabri, E Kristof and MI Artika. Effects of methods and durations of extraction on total flavonoid and phenolic contents and antioxidant activity of java cardamom (*Amomum compactum* Soland Ex Maton) fruit. *Plants* 2022; **11(17)**, 2221.

[16] Fitriani, A Karim and HA Wardani. Determination of total tannin content of temulawak rhizomes (*Curcuma xanthorrhiza* Roxb) in various boiling time variations using UV-Vis spectrophotometry method. *Journal Pharmacy of Pelamonia* 2023; **3(1)**, 47-52.

[17] S Wahyuni and MP Marpaung. Determination of total alkaloid levels extracts of akar kuning (*Fibraurea chloreleuca* Miers) based on the differences of ethanol concentrations by spectrophotometry UV-Vis method. *Dalton* 2020; **3(2)**, 52-61.

[18] F Tunnisa, DN Faridah, A Afriyanti, D Rosalina, MA Syabana, N Darmawan and ND Yliana. Antioxidant and antidiabetic compounds identification in several Indonesian underutilized Zingiberaceae spices using SPME-GC/MS-based volatilomics and *in silico* methods. *Food Chemistry X* 2022; **14**, 100285.

[19] UMS Purwanto, K Aprilia and Sulistiyani. Antioxidant activity of telang (*Clitoria ternatea* L.) extract in inhibiting lipid peroxidation. *Current Biochemistry* 2022; **9(1)**, 26-37.

[20] BFD Zaelani, M Safithri and D Andrianto. *In vitro* study of *Piper crocatum* Ruiz & Pav potency as HMG-CoA reductase and malondialdehyde formation inhibitor. *Indonesian Journal of Applied Research* 2024; **5(3)**, 185-195.

[21] EW Purnama, M Safithri and D Andrianto. Clusterization of red betel leaves (*Piper crocatum*) from various regions in Indonesia based on secondary metabolite fingerprint analysis and cytotoxicity values. *Indonesian Journal of Applied Research* 2023; **4(2)**, 170-182.

[22] EYY Nurinsani, D Andrianto and M Safithri. Acetylcholinesterase inhibition activity and phytochemical screening of red betel leaf (*Piper crocatum* Ruiz & Pav as anti-dementia agents. *BIO Web of Conferences* 2024; **123**, 02009.

[23] SK Whardhani, S Abdillah and R Djamil. Acetylcholinesterase inhibition and determination of quality parameters polyherbal and combination extracts from *Moringa oleifera* Lam., *Phyllanthus niruri* L., and *Nigella sativa* L. *Health Science Journal of Indonesia* 2023; **14(2)**, 57-64.

[24] MO Hassan and RA Mohamed. *In-silico* screening for potential natural compounds against acetylcholinesterase, causing Alzheimer disease. *International Journal of Agriculture, Forestry and Plantation* 2024; **15**, 65-68.

[25] RAP Irsal, GM Gholam, MA Dwicesaria, TF Mansyah and F Chairunisa. Exploring the potential of *Scabiosa columbaria* in Alzheimer's disease treatment: An *in silico* approach. *Journal of Taibah University Medical Sciences* 2024; **19(5)**, 947-960.

[26] CPM da Silva, GM das Neves, GLV Poser, VL Eifler-Lima and SMK Rates. *In silico* prediction of ADMET/drug-likeness properties of bioactive phloroglucinols from *Hypericum* gents. *Medicinal Shemistry* 2023; **19(10)**, 1002-1017.

[27] Indriati, F Jalung and F Umamy. Determination of curcumin levels in *Curcuma xanthorrhiza* rhizome extract with maceration and remaceration techniques. *Journal of Pharmaceutical and Sciences* 2022; **5(2)**, 505-510.

[28] FM Lubis, AS Daulay, HM Nasution and Ridwanto. Optimization of modified corn flour production based on protein content through fermentation with lactic acid bacteria (LAB). *Journal of Health and Medical Science* 2022; **1(3)**, 219-229.

[29] A Karim, D Ma'ruf and R Haeruddin. Uji efektivitas fraksi ekstrak etanol rimpang temulawak (*Curcuma zanthorrhiza* Roxb) dari Kabupaten Takalar sebagai antibakteri terhadap *staphylococcus aureus* (*in Indonesian*). *Journal Pharmacy of Pelamonia* 2024; **4(2)**, 97-102.

[30] I Widyastuti, HZ Kuthfah, YI Hartono, R Islamadina, AT Can and A Rohman. Antioxidant activity of temulawak (*Curcuma xanthorrhiza*

Roxb.) and its classification with chemometrics. *Indonesian Journal of Chemometric and Pharmaceutical Analysis* 2021; **1(1)**, 29-42.

[31] I El Mannoubi. Impact of different solvents on extraction yield, phenolic composition, *in vitro* antioxidant and antibacterial activities of deseeded *Opuntia stricta* fruit. *Journal of Umm Al-Qura University for Applied Sciences* 2023; **9(2)**, 176-184.

[32] Suryani, AC Al Anshory, IM Artika, L Ambarsari and W Nurcholis. Variability total phenolic content and antioxidant activity of *Curcuma zanthorrhiza* and *C. aeruginosa* cultivates in three different locations in West Java, Indonesia. *Biodiversitas* 2022; **23(4)**, 1998-2003.

[33] NS Ngadirin, R Hasham, NJ Sulaiman and NHM Ariffin. Effect of *Curcuma xanthorrhiza* extract on the phytochemical content, antioxidant activity and *Lactobacillus casei* growth. *Bioprocessing and Biomass Technology* 2024; **3(1)**, 7-11.

[34] YSW Manuhara, S Sugiharyo, AN Kristanti, NS Aminah, AT Wibowo, AP Wardana, YK Putro and D Sugiarso. Antioxidant activities, total phenol, flavonoid, and mineral content in the rhizome of various Indonesian herbal plants. *Rasayan Journal of Chemistry* 2022; **15(4)**, 2724-2730.

[35] Z Haida, S Ab Ghani and M Hakiman. Extraction variables optimization on phenolics content and antioxidant activities of *in-vitro* propagated leaves of *Curcuma caesia* Roxb. using response surface methodology. *BioResources* 2025; **20(2)**, 4590-4607.

[36] S Kartini, S Juariah, D Mardhiyani, MFA Bakar, FIA Bakar and S Endrini. Phytochemical properties, antioxidant activity and α-amilase inhibitory of *Curucuma caesia*. *Journal of Advanced Research in Applied Sciences and Engineering Technology* 2023; **30(1)**, 255-263.

[37] V Isha, K Venkatesan, V Rajashree, N Senthil, R Renuka and K Chandrakumar. Evaluation of phytochemical variations among the different genotypes of black turmeric (*Curcuma caesia* Roxb.). *Biochemical Genetics* 2025. https://doi.org/10.1007/s10528-025-11304-y

[38] R Asyhar, M Minarni, RA Arista and W Nurcholis. Total phenolic and flavonoid contents and their antioxidant capacity of *Curcuma xanthorrhiza* accessions from Jambi. *Biodiversitas* 2023; **24(9)**, 5007-5014.

[39] G Yodi, IM Artika and W Nurcholis. Effect of varieties of *Curcuma xanthorrhiza* and extraction solvent on total phenolic, total flavonoid content, and antioxidant capacity. *Biodiversitas* 2023; **24(12)**, 6425-6431.

[40] H Gul and E Nakilcioğlu. Proces optimization of bioactive compounds extraction from bee bread using deep eutectic solvents: A response surface methodology approach. *Journal of Food Measurement and Characterization* 2026. https://doi.org/10.1007/s11694-025-04019-6

[41] A Jain, P Jain, S Bajaj, A Majumdar and P Soni. Chemoprofiling and antioxidant activity of edible curcuma species. *Food and Humanity* 2023; **1**, 1027-1039.

[42] L Suhendra. Antioxidant activity of turmeric powder extract (*Curcuma domestica* Val.). *Agrotechno* 2017; **2(2)**, 237-247.

[43] H Kusriani, Y Mulyani, R Santoso, G Jafar, FZ Ishmah and NA Zahra. Pharmacological assessment of standardized *Curcuma longa* L. and *Centella asiatica* (L.) urban extracts for diabetes management. *Journal of Pharmacy & Pharmacognosy Research* 2026; **14(1)**, 2290.

[44] D Davis, D Trisciuzzi, R Sreekumar, MB Jacob, K Madhu, N Gambacorta, M Catto, DGT Parambi, O Nicolotti and B Mathew. Key chemotypes for the rational design of dual AChE/BACE-1 inhibitors. *Current Medicinal Chemistry* 2026; **33(1)**, 23-41.

[45] P Pooladgar, M Sakhabkhsh, A Taghva and S Soleiman-Meigooni. Beyond alzheimer's disease? A narrative review of therapeutic potentials of donepezil in different diseases. *Iranian Journal of Pharmaceutical Research* 2022; **21(1)**, e128408.

[46] TA Rants'o, DG van Greunen, CJ van der Westhuizen, DL Riley, JL Panayides, LL Koekemoer and RL van Zyl. The *in silico* and *in vitro* analysis of donepezil derivatives for *Anopheles* acetylcholinesterase inhibition. *PLoS One* 2022; **17(11)**, e0277363.

[47] D Drozdowska, D Maliszewski, A Wróbel, A Ratkiewicz and M Sienkiewicz. New benzamides as multi-targeted compounds: synthesis, AChE and BACE1 inhibitory activity, and molecular

docking study. *International Journal of Molecular Sciences* 2023; **24(19)**, 14901.

[48] Z Mahmoud, HS Sayed, LW Mohamed and KO Mohamed. Development of new donepezil analogs: Synthesis, biological screening, and *in silico* study rationale. *Medicinal Chemistry Research* 2022; **31**, 1754-1770.

[49] A Perez, HA Martinez-Correa, F Parada-Alfonso, ZJS Montenegro, D Ballesteros-Vivas, G Álvarez-Rivera, A Cifuentes and E Ibáñez. Antioxidant, neuroprotective and anti-inflammatory activity of *Curcuma longa*: From green extraction to nanoemulsion. *Frontiers in Nutrition* 2025; **12**, 1619725.

[50] AV Deepa and TT Dennis. Plant extracts and phytochemicals targeting Alzheimer's disease through acetylcholinesterase inhibition. *Exploration of Neuroscience* 2025; **4**, 100697.

[51] ME Klau, E Rohaeti, M Rafi, IM Artika, L Ambarsari and W Nurcholis. Metabolite profiling of *Curcuma zanthorrhiza* varieties grown in different regions using UHPLC-Q-Orbitrap-HRMS and chemometrics analysis. *Biointerface Research in Applied Chemistry* 2023; **13(1)**, 26.

[52] AS Anggraeni, A Windarsih, HD Warmiko, A Rohman, Suratno, AA Styawan and A Widarti. Non-targeted metabolomics analysis of *Curcuma* rhizomes species from different origins using LC-orbitrap HRMS combined with chemometrics. *Ecology* 2026; **124**, 105140.

[53] R Budhathoki, AP Timilsina, BP Regmi, KR Sharma, N Aryal and N Parajuli. Metabolome mining of *Curcuma longa* L. using HPLC-MS/MS and molecular networking. *Metabolites* 2023; **13(8)**, 898.

[54] L Yu, N Li, B Li, KX Ye, J Guo, J Shan, L Cao, M Song, Y Wang, T Lee, AB Maier and L Feng. Targeting cognitive aging with curcumin supplementation: A systematic review and meta-analysis. *The Journal of Prevention of Alzheimer's Disease* 2025; **12(8)**, 100248.

[55] A Lechoczki, M Fekete, T Jarecsny, V Zábó, Á Szappanos, T Csípő, Á Lipécz, M Major, V Fazekas-Pongor, P Varga and JT Varga. The neuroprotective role of curcumin: From molecular pathways to clinical translation-a narrative review. *Nutrients* 2025; **17(17)**, 2884.

[56] A Simamora, KH Timotius, H Setiawan, FA Saputri, CR Putri, D Aryani, RA Ningrum and A Mun'im. Ultrasonic-assisted extraction of xanthorrhizol from *Curcuma xanthorrhiza* Roxb. Rhizomes by natural deep eutectic solvents: optimization, antioxidant activity, and toxicity profiles. *Molecules* 2024; **29(9)**, 2093.

[57] VUM Nallal, R Padmini, B Ravindran, SW Chang, R Radhakrishman, HSM Almoallim, SA Alharbi and M Razia. Combined *in vitro* and *in silico* approach to evaluate the inhibitory potential of an underutilized allium vegetable ad its pharmacologically active compounds on multidrug resistant Candida species. *Saudi Journal of Biological Sciences* 2021; **28(2)**, 1246-1256.

[58] HK Nivatya, A Singh, N Kumar, Sonam, L Sharma, V Singh, R Mishra, N Gaur and AK Mishra. Assessing molecular docking tools: understanding drug discovery and design. *Future Journal of Pharmaceutical Sciences* 2025; **11(11)**, 111.

[59] F Az-Zahra, J Afidika, SDA Diamantha, AE Rahmani, S Fatimah, DL Aulifa, AA Elaine and BDP Sitinjak. Studi *in silico* senyawa dalam daun sirih (*Piper betle* L.) sebagai inhibitor enzim asetilkolinesterase (AChE) pada penyakit Alzheimer (*in Indonesian*). *Indonesian Journal of Biological Pharmacy* 2022; **2(2)**, 44-58

[60] M Safithri, EB Koendhori, D Andrianto, R Kurniasih, MA Dwicesaria, EYY Nurinsani, MA Umar and M Hufdayanti. Analysis of bioactive compounds *Piper crocatum* as inhibitors of acetylcholinesterase *in silico* and *in vitro*. *Trends in Sciences* 2025; **22(4)**, 9437.

[61] M Atanasova, I Dimitrov, S Ivanov, B Georgiev, S Berkov, D Zheleva-Dimitrova and I Doytchinova. Virtual screening and hit selection of natural compounds as acetylcholinesterase inhibitors. *Molecules* 2022; **27(10)**, 3139.

[62] S Peitzika and E Pontiki. Recent approaches in molecular docking studies of novel compounds targeting acetylcholinesterase in Alzheimer's disease. *Molecules* 2023; **28(3)**, 1084.

[63] MF Reynoso-García, DE Nicolás-Álvarez, AY Tenorio-Barajas and A Reyes-Chaparro. Structural bioinformatics applied to

acetylcholinesterase enzyme inhibition. *International Journal of Molecular Sciences* 2025; **26(8)**, 3781.

[64] M Makarian, M Gonzalez, SM Salvador, S Lorzadeh, PK Hudson and S Pecic. Synthesis, kinetic evaluation and molecular docking studies of donepezil-based acetylcholinesterase inhibitors. *Journal of Molecular Structure* 2022; **1247**, 131425.

[65] M Jain, R Dhariwal, K Bhardava, S Das, M Shaikh, R Tendulkar, R Wani, M Sharma, AK Delta and P Kaushik. *In silico* and *in vitro* profiling of curcumin and its derivatives as potent acetylcholinesterase inhibitors. *Biocatalysis and Agricultural Biotechnology* 2024; **56**, 103022.

[66] E Salamanova, M Atanasova, I Doytchinova. A novel galantamine-curcumin hybrid inhibits butyrylcholinesterase: A molecular dynamics study. *Chemistry* 2024; **6(6)**, 1645-1657.

[67] SA Kehinde, WP Lin, BB Lay, KY Phyo, MM San, R Pattanayaiying and S Chusri. Curcumin and dementia: A systematic review of its effects on oxidative stress and cognitive outcomes in animal models. *International Journal of Molecular Sciences* 2025; **26(14)**, 7026.

[68] H Hussain, S Ahmad, SWA Shah, M Ghias, A Ullah, SU Rahman, Z Kamal, FA Khan, NM Khan, J Muhammad, M Almehmadi, O Abdulaziz and S Alghamdi. Neuroprotective potential of synthetic monocarbonylic curcumin analogs assessed by molecular docking studies. *Molecules* 2021; **26(23)**, 7168.

[69] SLS Min, SY Liew, NJY Chear, BH Goh, WN Tan and KY Khaw. Plant terpenoids as a promising source of cholinesterase inhibitors for anti-Alzheimer therapy. *Biology* 2022; **11(2)**, 307.

[70] A Jaśkiewicz, G Budryn, M Carmena-Bargueño and H Pérez-Sánchez. Evaluation of sesquiterpene lactones and chicory extracts as acetylcholinesterase inhibitors using calorimetric and docking simulation studies. *Nutrients*. 2022; **14(17)**, 3633.

[71] N Smyrska-Wieleba and T Mroczek. Natural inhibitors of cholinesterases: Chemistry, structure–activity relationships and analytical methods. *International Journal of Molecular Sciences* 2023; **24(3)**, 2722.

[72] A Arya, R Chahal, R Rao, MH Rahman, D Kaushik, MF Akhtar, A Saleem, SMA Khalifa, HR El-Seedi, M Kamel, GM Albadrani, MM Abdel-Daim and V Mittal. Acetylcholinesterase inhibitory potential of sesquiterpene analogues for Alzheimer's disease therapy. *Biomolecules* 2021; **11(3)**, 350.

[73] G Xiong, Z Wu, J Yi, L Fu, Z Yang, C Hsieh, M Yin, X Zeng, C Wu, A Lu and others. ADMETlab 2.0: An integrated online platform for accurate and comprehensive ADMET property prediction. *Nucleic Acids Research* 2021; **49(W1)**, W5-W14.

[74] A Bayraktar, X Li, W Kim, C Zhang, H Turkez, S Shoaie and A Mardinoglu. Drug repositioning targeting glutaminase reveals drug candidates for the treatment for Alzheimer's disease patients. *Journal of Translational Medicine* 2023; **21**, 332.

[75] DC Negru, SG Bungau, A Radu, DM Tit, A Radu, DC Nistor-Cseppento and PA Negru. Evaluation of alkaloids as inhibitors of human acetylcholinesterase using molecular docking and ADME prediction. *In Vivo* 2025; **39**, 236-250.

[76] AS Singh and C Vellapandian. *In silico* and pharmacokinetic assessment of echinocystic acid in Alzheimer's disease-like pathology. *Future Science OA* 2023; **10(1)**, FSO904.

[77] B Ghorbani-nejad, M Baghani, S Amiri, NA Delche, MH Darijani, M Soltani, A Nezami and M Rahimzadegan. Curcumin: Multifaceted biological actions and therapeutic implications - a narrative review. *Inflammopharmacology* 2025; **33**, 6309-6327.

[78] M Mujtaba, F Ahmad and M Fatima. *In silico* evaluation of daechulalkaloid A maltoxazine as a potential acetylcholinesterase inhibitor for Alzheimer's disease. *PHYTONutrients* 2025; **4(1)**, 44-56.

[79] U Kochman, H Sitka, J Kuźniar, M Czaja, P Kozubek, JA Beszłej, J Leszek. Targeted nanoparticles for drug delivery across the blood-brain barrier in early and late stages of Alzheimer's disease: A review. *Molecular Neurobiology* 2025; **63(1)**, 75.

[80] TA Rants'o, DG van Greunen, CJ van der Westhuizen, DL Riley, JL Panayides, LL Koekemoer and RL van Zyl. The *in silico* and *in vitro* analysis of donepezil derivatives for

Anopheles acetylcholinesterase inhibition. *PLoS One* 2022; **17(11)**, e0277363.

[81] HMA Hasan, HAA Khalid and F Abdulsayid. Infrared characterization and physicochemical properties of a Schiff base compound synthesized from 4-hydroxy-3-methoxybenzaldehyde and 2-amino-3-methylbutanoic acid. *Journal of Research in Pharmacy and Sciences* 2021; **7(3)**, 8-12.

[82] N Anand, NN Quailes, MN Szobody and B Gadad. Simulations of physicochemical and ADMET properties of curcumin and its derivatives. *Journal of Pharmacology and Experimental Therapeutics* 2025; **392(3)**, 103481.

[83] J Kuzminska, P Szyk, DT Mlynarczyk, P Bakun, I Muszalska-Kolos, K Dettlaff, A Sobczak, T Goslinski and A Jelinska. Curcumin derivatives in medicinal chemistry: Potential applications in cancer treatment. *Molecules* 2024; **29(22)**, 5321.

[84] J Khwarg, H Lee, K Yu, E Seol and J Chung. Population pharmacokinetic modeling and simulation for dose optimization of GB-5001, a long-acting intramuscular injection of donepezil, in healthy participants. *Neurological Therapy* 2024; **13**, 1453-1466.

[85] R Prasetiawati, M Suherman, B Permana and Rahmawati. Molecular docking study of anthocyanidin compounds against epidermal growth factor receptor as anti-lung cancer agents. *Indonesian Journal of Pharmaceutical Science and Technology* 2021; **8(1)**, 8-20.

[86] E Park, E Kim, K Kim, J Jeon, I Song, S Park and K Li. Revisiting donepezil metabolism in rats using non-targeted metabolomics and molecular networking. *Pharmaceutics* 2025; **17(1)**, 115.

[87] J Lee, JL Beers, RM Geffert and KD Jackson. CYP-mediated drug interactions: Mechanisms and *in vitro* assessment. *Biomolecules* 2024; **14(1)**, 89.

[88] D Klimoszek, M Jeleń, M Dołowy and B Morak-Młodawska. Lipophilicity and ADMET parameters of new anticancer diquinothiazines. *Pharmaceuticals* 2024; **17(6)**, 725.

[89] MJ Ratain and WK Plunkett. *Principles of pharmacokinetics*. *In*: DW Kufe, RE Pollock, RR Weichselbaum, RC Bast, TS Gansler, JF Holland and E Frei (Eds.). Holland-Frei Cancer Medicine. 6th ed. BC Decker, Ontario, Canada, 2003.

[90] Y Myung, AGC de Sá and DB Ascher. Deep-PK: Deep learning for small-molecule pharmacokinetic and toxicity prediction. *Nucleic Acids Research* 2024; **52(W1)**, W469-W475.

[91] EV Stolaki, K Psatha and M Aivaliotis. Metabolomics and pharmacometabolomics: Advancing Precision Medicine in Drug Discovery and Development. *Metabolites* 2025; **15(11)**, 750.

[92] N Fan, J Chen, J Wang, ZS Chen and Y Yang. Bridging data and drug development: Machine learning approaches for next-generation ADMET prediction. *Drug Discovery Today* 2025; **30(11)**, 104487.